Attribution of the Australian bushfire risk to anthropogenic climate change

Geert Jan van Oldenborgh[1], Folmer Krikken[1], Sophie Lewis[2], Nicholas J. Leach[3], Flavio Lehner[4,5,6], Kate R. Saunders[7], Michiel van Weele[1], Karsten Haustein[8], Sihan Li[8,9], David Wallom[9], Sarah Sparrow[9], Julie Arrighi[10,11], Roop P. Singh[10], [10,12,13], Sjoukje Y. Philip[1], Robert Vautard[14], and Friederike E. L. Otto[8]

[1]Royal Netherlands Meteorological Institute (KNMI), De Bilt, Netherlands
[2]University of New South Wales, Canberra, ACT, Australia
[3]Atmospheric, Oceanic and Planetary Physics, Department of Physics, University of Oxford, Oxford, U.K.
[4]Department of Earth and Atmospheric Sciences, Cornell University, Ithaca, USA
[5]Institute for Atmospheric and Climate Science, ETH Zürich, Zürich, Switzerland
[6]Climate and Global Dynamics Laboratory, National Center for Atmospheric Research, Boulder, USA
[7]Delft Institute of Applied Mathematics, Delft University of Technology, Delft, Netherlands
[8]Environmental Change Institute, University of Oxford, Oxford, U.K.
[9]Oxford e-Research Centre, University of Oxford, Oxford, U.K.
[10]Red Cross Red Crescent Climate Centre, The Hague, Netherlands
[11]Global Disaster Preparedness Center, Washington DC, USA
[12]Faculty of Geo-information Science and Earth Observation, University of Twente, Enschede, Netherlands
[13]International Research Institute for Climate and Society, Columbia University, New York, USA
[14]Institut Pierre-Simon Laplace, France

Correspondence: G. J. van Oldenborgh (oldenborgh@knmi.nl)

Abstract. Disastrous bushfires during the last months of 2019 and January 2020 affected Australia, raising the question to what extent the risk of these fires was exacerbated by anthropogenic climate change. To answer the question for southeastern Australia, where fires were particularly severe, affecting people and ecosystems, we use a physically-based index of fire weather, the Fire Weather Index, long-term observations of heat and drought, and eleven large ensembles of state-of-the-art climate models. We find large trends in the Fire Weather Index in the ERA5 reanalysis since 1979, and a smaller but significant increase by at least 30% in the models. Therefore, we find that climate change has induced a higher weather-induced risk of such an extreme fire season. This trend is mainly driven by the increase of temperature extremes. In agreement with previous analyses we find that heat extremes have become more likely by at least a factor of two due to the long-term warming trend. However, current climate models overestimate variability and tend to underestimate the long-term trend in these extremes, so the true change in the likelihood of extreme heat could be larger, suggesting that the attribution of the increased fire weather risk is a conservative estimate. We do not find an attributable trend in either extreme annual drought or the driest month of the fire season September–February. The observations, however, show a weak drying trend in the annual mean. ~~Finally, we find large trends in the Fire Weather Index in the ERA5 reanalysis, and a smaller but significant increase by at least 30% in the models. The trend is mainly driven by the increase of temperature extremes and hence also likely underestimated.~~ For the 2019/20 season more than half of the July–December drought was driven by record excursions of the Indian Ocean dipole and

Southern Annular Mode. These factors , factors which are included in the analysis here. The study reveals the complexity of the 2019/20 bushfire event, with some, but not all drivers showing an imprint of anthropogenic climate change. Finally, the study concludes with a qualitative review of various vulnerability and exposure factors that each play a role, along with the hazard, in increasing or decreasing the overall impact of the bushfires.

1 Introduction

2019 was the warmest and driest year in Australia since homogeneous standardized temperature and rainfall observations began (in 1910 and 1900), following two already dry years in large parts of the country. These conditionsas well as a strong , driven partly by a strong positive Indian Ocean Dipole from the middle of the year onwards and a large-amplitude negative excursion of the Southern Annular Mode, led to weather conditions conducive to bushfires across the continent and so the annual bushfires were more widespread and intense and started earlier in the season than usual (Bureau of Meteorology, Annual Climate Statement 2019). There was unprecedented The bushfire activity across the states of Queensland (QLD), New South Wales (NSW), Victoria (VIC), South Australia (SA), Western Australia (WA) and in the Australian Capital Territory (ACT) was unprecedented in terms of the area burnt in densely populated regions.

In addition to the unprecedented nature of this event, its impacts to date have been disastrous (Reliefweb Australia: bushfires, 2020). There have been at least 34 fatalities as a direct result of the bushfires and the resulting smoke caused hazardous air quality adversely affected millions of residents in cities in these regionswith levels higher than twenty times those considered safe by the Australian government. About 5,900 buildings have been destroyed. There are estimates that between 0.5 and 1.5 billion wild animals lost their lives, along with tens of thousands of livestock. The bushfires are having an economic impact (including millions in insurance claimssubstantial insurance claims, e.g., PERILS press release), as well an immediate and long term health impact to the people exposed to smoke and dealing with the psychological impacts of the fires (Finlay et al., 2012) .

It has at times been difficult for emergency services to protect or evacuate some communities due to the pace at which the bushfires have spread, sometimes forcing residents to flee to beaches and lakes to await rescue. Interruptions of the supply of power, fuel and food supplies have been reported and road closures have been common. This has resulted in total isolation of some communities, or only accessible by air or sea when smoke conditions allow . The long and severe drought during 2019 and the two years before is expected to have a strong negative impact on agriculture (Reliefweb Australia: bushfires, 2020).

It is well-established that wildfire smoke exposure is associated with respiratory morbidity (Reid et al., 2016). Additionally, fine particulate matter in smoke may act as a triggering factor for acute coronary events (such as heart attack-related deaths) as found for previous fires in southeast Australia (Haikerwal et al., 2015). As noted by Johnston and Bowman (2014), increased bushfire-related risks in a warming climate have significant implications for the health sector, including given measurable increases in illness, hospital admissions, and deaths associated with severe smoke events.

Based on the recovery of areas following previous major fires, such as Black Saturday in Victoria in 2009, these impacts are likely to affect people, ecosystems and the region for a substantial period to come.

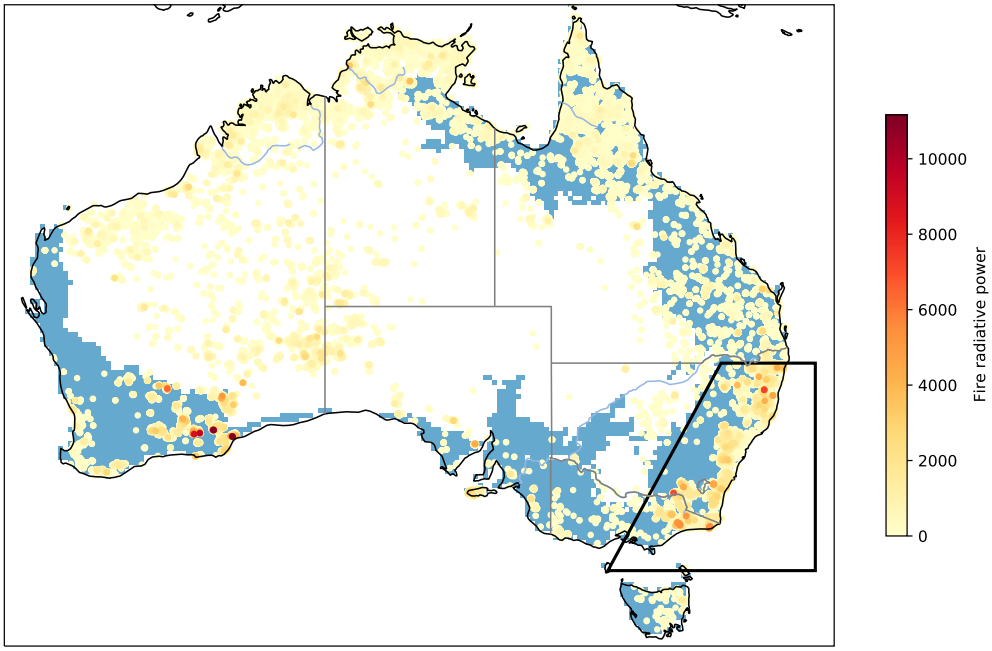

Figure 1. ~~Modis~~ Moderate Resolution Imaging Spectroradiometer (MODIS) active fire data (Collection 6, near real time and standard products) showing the severity of bushfires from 1 ~~July~~ October 2019 to 10 January 2020 with the most severe fires being depicted in red. The image also shows the forested areas ~~of Eastern Australia~~ in blue. The polygon shows the area analysed in this article.

The satellite image in Fig. 1 shows the severity of the fires ~~since July, with~~ between October, illustrating two regions with particularly severe events in the South West and South East. ~~Due to the fact that in the South East many population centres were affected and the region was also strongly affected by drought we focus our analysis on~~ We focus our analysis on the South East due to the affected population centres and the concomitant drought in this region. The grass fires in the non-forested areas have completely different characteristics and are not considered here.

Wildfires in general are one of the most complex weather-related extreme events (Sanderson and Fisher, 2020) with their occurrence depending on many factors including the weather conditions conducive to fire at the time of the event and also on the availability of fuel, which in turn depends on rainfall, temperature and humidity in the weeks, months and sometimes even years preceding the actual fire event. In addition, ignition sources and type of vegetation as factors largely ~~outside the~~ independent of meteorology play an important role. In this analysis we only consider the influence of weather and climate on the fire risk, excluding ignition sources and weather caused by the fires such as pyrocumunimbus development. There is ~~not one~~ no unified definition of what fire weather consists of as the relative importance of different factors depends on the climatology of the region. For instance, fires in grasslands in semi-arid regions behave very differently than those in temperate forests. There are a few key meteorological variables that are important: temperature, precipitation, humidity and wind (speed as well as direction). Fire danger indices are derived from these variables either using physical models or empirical relationships between these variables and fire occurrence, including observed factors such as the rate of spread of fires and measurements of fuel moisture content with different sets of weather conditions.

Southeast Australia experiences a temperate climate and on the eastern seaboard hot summers are interspersed with intense rainfall events, often linked with 'east-coast lows' (Pepler et al., 2014). Bushfire activity historically commences in the Austral spring (September-November) in the north and summer (December-February) in the south (Clarke et al., 2011). In Australia the Forest Fire Danger Index ~~(FFDI McArthur, 1966, 1967; Noble et al., 1980)~~ (FFDI, McArthur, 1966, 1967; Noble et al., 1980) is commonly used for indicating dangerous weather conditions for bushfires, including for issuing operational forecasts during the 2019/20 summer. The index is based on temperature, humidity and wind speed on a given day as well as a drought-factor which is based on antecedent temperature and rainfall. ~~Southeast Australia experiences a temperate climate and on the eastern seaboard hot summers are interspersed with intense rainfall events, often linked with 'east-coast lows' (Pepler et al., 2014). Bushfire activity historically commences in the Austral spring (September-November) in the north and summer (December-February) in the south Clarke et al. (2011). Bushfire~~

Bushfire weather risk, as characterised by the FFDI, has increased across much of Australia in recent decades (Clarke et al., 2013; Dowdy, 2018; Harris and Lucas, 2019). Similar, increasing trends in fire weather conditions over southern Australia have been identified in other studies, both for the FFDI (e.g., Dowdy, 2018) and for indices representing pyroconvective processes (Dowdy and Pepler, 2018). These observed trends over southeast Australia are broadly consistent with the projected impacts of climate change (e.g., Clarke et al., 2011; Dowdy et al., 2019). For individual fire events, studies have shown that it can be difficult to separate the influence of anthropogenic climate change from that of natural variability (e.g., Hope et al., 2019; Lewis et al., 2019).

An alternative index is the physically based Canadian Fire Weather Index (FWI) that also includes the influence of wind on the fuel availability (Dowdy, 2018). The latter is achieved by modelling fuel moisture on three different depths including the influence of humidity and wind speed on the upper fuel layer (Krikken et al., 2019). While the FWI was originally developed specifically for the Canadian forests, the physical basis of the models allows it to be used for many different climatic regions of the world (e.g., Camia and Amatulli, 2009; Dimitrakopoulos et al., 2011), and has been shown to provide a good indication of the occurrence of previous extreme fire events in the ~~South Eastern~~ Southeastern Australian climate (Dowdy et al., 2009). A study on the emergence of the fire weather anthropogenic signal from noise indicated that this is expected around 2040 for Southern Australia (Abatzoglou et al., 2019) using the FWI. In this study we also consider the Monthly Severity Rating (MSR), which is derived from the FWI and reflects better how difficult a fire is to suppress (Shabbar et al., 2011). A more detailed analysis of the FWI in the context of bushfires in southeastern Australia is given in section 2.1.

As the fire risk indices depend on heat and drought ~~,~~and these were also extreme in 2019/2020, we also consider these factors separately. Previous attribution studies on Australian extreme heat at regional scales ~~has~~ have generally indicated an influence from anthropogenic climate change. The 'angry summer' of 2012/2013—which until 2018/2019 was the hottest summer on record—was found to be at least 5 times more likely to occur due to human influence (Lewis and Karoly, 2013). The frequency and intensity of heatwaves during this summer were also found to increase (Perkins et al., 2014). Other attribution assessments that found an attributable influence on extreme Australian heat include the May 2014 heatwave (Perkins and Gibson, 2015), the record October heat in 2015 (Hope et al., 2016), and extreme Brisbane heat during November 2014 (King et al., 2015a). However, at small spatial scales~~such as in-situ sites~~, human influence on extreme heat is ~~less clear~~ sometimes less clear, as in Melbourne in January 2014 (Black et al., 2015). It is worth noting that Lewis et al. (2019) found that the temperature component of the extreme 2018 Queensland fire weather had an anthropogenic influence, while no clear influence was detected on the February 2017 extreme fire weather over Eastern Australia (Hope et al., 2019). We are not aware of any extreme event attribution studies on Australian drought.

Thus, while it is clear that climate change does play an important role in heat and fire weather risk overall, assessing the magnitude of this risk and the interplay with local factors has been difficult. Nevertheless it is crucial to prioritise adaptation and resilience measures to reduce the potential impacts of rising risks.

We perform the analysis of possible connections between the fire weather risk and anthropogenic climate change in three steps. First, we assess the trends in extreme temperature and conduct an attribution study using ~~a~~ the annual maximum of the seven-day moving average of ~~annual~~ daily maximum temperatures corresponding to the time scale chosen for the ~~Fire Weather Index~~FWI (Section 3). Second, we undertake the same analysis but for ~~drought defined as purely~~ meteorological drought (i.e., defined purely as a lack of rainfall) in two time windows, the annual precipitation as well as the driest month ~~in~~ within the fire season, ~~with the~~ which is September–February in our study area (Section 4). The latter again roughly ~~corresponding to the input time scale of~~ corresponds to the time scale on which precipitation deficits factor into the FWI, namely 52 days. Third, and most importantly, we conduct an attribution study on the ~~Fire Weather Index (FWI) and the Monthly Severity Rating (MSR~~FWI and MSR as indices of the probability of bushfires due to the weather (Section 5). These three attribution studies follow the same protocol used in previous assessments~~(Heat~~: heat waves: Kew et al. (2019); low precipitation: Otto et al. (2018b); Fire Weather

Index: Krikken et al. (2019). ~~We continue the analysis with a~~ The full and generalized event attribution protocol has recently been documented in Philip et al. (2020). In order to condense the lengthy analysis, we provide short overviews of the heat and drought analysis in the main paper, with extensive results in the Supplementary Material, and focus primarily on the FWI and MSR analysis. We also provide a short analysis and discussion of other large scale drivers that were of potential importance during 2019/20, such as El Niño Southern Oscillation (ENSO), the Indian Ocean Dipole (IOD) or the Southern Annular Mode (SAM)~~. Finally we consider~~ , in Section 6.1 and a detailed analysis in the Supplementary Material, section S3. Finally, we briefly discuss non-climate factors~~(~~, such as exposure and vulnerability~~)~~ , that have contributed to the impacts of the extreme fire season of 2019/20.

2 Data and methods

2.1 ~~Event~~ General event definition

~~In this article we trace the connection between anthropogenic climate change and the likelihood and intensity of dangerous bushfire conditions as parametrised by the FWI in~~ Since we are investigating several different indicator or driver variables of fire risk, different event definitions are developed for different variables. The details of those definitions are given at the beginning of the respective sections on temperature, precipitation, and fire weather indices (Sections 3–5). General parameters of the event definition are given here.

The fire season (September–February) serves as the general event time window and the region with the most intense fires in 2019/20 in southeastern Australia ~~. We defined this region as the~~ serves as the general event spatial domain; specifically the land area in the polygon 29 °S, 155 °E; 29 °S, 150 °E; 40 °S, 144 °E and 40 °S, 155 °E (as shown in Fig. 1)~~. This corresponds with~~ , which corresponds to the area between the Great Dividing Range and the coast.

~~To capture the variations in the start of the fire season in the region described above we take for most quantities first the annual maximum per grid point over the fire season September–February and next the spatial average over the region defined above. This way the events do not need to be simultaneous at separate grid points within the region. We therefore investigate the question how~~ The primary way we investigate the connection between anthropogenic climate change ~~influences the chances of an intense bushfire season, rather than focusing on a single episode of intense bushfires.~~

~~The FWI Index~~ and the likelihood and intensity of dangerous bushfire conditions is through the FWI. The FWI provides a reasonable proxy for the burnt area in the extended summer months, with the strongest relationship observed from November to February. Fig. 2 shows both the Spearman rank ~~based~~ correlation and the Pearson correlation ~~when a log-transform of the burnt areawas taken~~of FWI with log-transformed burnt area. The 95% confidence intervals are also shown. Given the similarity in the confidence intervals, the log-linear relationship appears to explain equal variability to that of the ranks.

To capture spatial variations in the start of the fire season at a given location within the event domain, we take for most quantities first the maximum per grid point over the fire season (September–February) and next the spatial average over the general event domain. This way the events do not need to be simultaneous at separate grid points within the region. We therefore

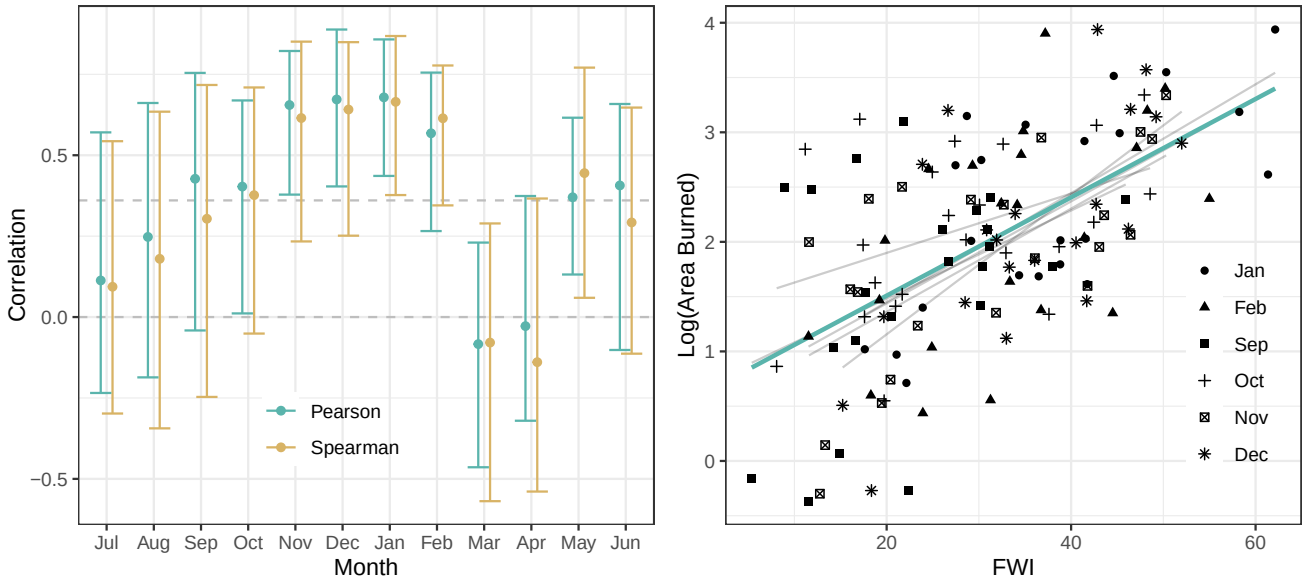

Figure 2. Left: correlation ~~and 95% two-sided interval based on~~ between the ~~bootstrap of the~~ logarithm of area burnt ($^{10}\log(\mathrm{km}^2)$, MODIS, Collection 6) in the ~~index area as a function of~~ event domain and the 7-day maximum Fire Weather Index for each month of the year. The ~~horizontal line denotes~~ correlations are based on the ~~one-sided~~ years 1997 to 2018 and the 95% two-sided confidence interval ~~around~~ is based on bootstrapping those years. The horizontal line denotes the 5% significance critical value for a one-sided test of the null hypothesis that the correlation is zero against the alternative hypothesis that the correlation is positive. Right: scatterplot and regression line of the values for each month of the fire season ~~,~~ (September–February). The ~~correlations are based on~~ grey lines denote the ~~years 1997 to 2018~~ regression lines for the individual months, the green line for all months in the fire season.

investigate the question how anthropogenic climate change influences the chances of an intense bushfire season, rather than focusing on a single episode of intense bushfires.

In most years only very small areas are burnt, but the observational record also includes events with extremely large areas. Given this, we checked if the ~~burned~~ burnt area observations were heavy-tailed (Pasquale, 2013). We found that monthly ~~burned~~ burnt area was not Pareto-distributed and instead is reasonably approximated using a log-normal distribution. This supports using the log-transformation and extrapolating this relationship to the 2019/20 fire season. Temporal detrending of the observations did not alter these conclusions.

2.2 Observational data

The observational data used in this study are described in ~~Sect. ??, ??~~ Sections S1, S2 and 5.3 for heat, drought and the fire weather index respectively, including justifications for including or excluding certain datasets for certain research questions. For the Global Mean Surface temperature (GMST) we use GISTEMP surface temperature (Hansen et al., 2010).

name	context	resolution	members	time	reference
~~ASF20C~~ ASF-20C	seasonal hindcasts	T255L91 (0.71°)	51	1901–2010	Weisheimer et al. (2017)
CanESM2	CMIP5	2.8°	50	1950–2099	Kirchmeier-Young et al. (2017)
CESM1-CAM5	CMIP5	1°	40	1920–2100	Kay et al. (2015)
CSIRO-Mk3-6-0	CMIP5	1.9°	30	1850–2100	Jeffrey et al. (2013)
EC-Earth	CMIP5	T159 (1.1°)	16	1860–2100	Hazeleger et al. (2010)
GFDL-CM3	CMIP5	2.0°	20	1920–2100	Sun et al. (2018)
GFDL-ESM2M	CMIP5	2.0°	30	1950–2100	Rodgers et al. (2015)
HadGEM3-A	attribution	N216 (0.6°)	15	1960–2015	Ciavarella et al. (2018)
IPSL-CM6A-LR	CMIP6	2.5×1.5°	32	1950–2019	Boucher et al. (2020)
MPI-ESM	CMIP5	1.9°	100	1850–2099	Maher et al. (2019)
weather@home	attribution	N96 (1.8°)	1520 × 2	1987–2017	Guillod et al. (2017)

Table 1. List of climate model ensembles used.

2.3 Model and experiment descriptions

Attributing observed trends to anthropogenic climate change can only be done with physical climate models as they allow isolating different drivers. For this purpose we ~~use a large~~ included as large a set of ocean-atmosphere coupled ~~climate models~~and atmosphere-only (i.e., sea surface temperature (SST) prescribed) climate model ensembles as we could find within the time constraints of this study in order to obtain estimates of both the uncertainty due to natural variability and the model uncertainty. A selection of large ensembles of ~~CMIP5 models~~ climate models from the Coupled Model Intercomparison Project Phase 5 (CMIP5) has been used: CanESM2, CESM1-CAM5, CSIRO Mk3.6.0, EC-Earth 2.3, GFDL CM3, GFDL ESM2M and MPI ESM. In addition, the HadGem3-A N216 attribution model developed in the ~~EUCLEIA~~ EUropean CLimate and weather Events: Interpretation and Attribution (EUCLEIA) project, the weather@home distributed attribution project model and the ~~ASF20C~~ Atmospheric Seasonal Forecasts of the Twentieth Century (ASF-20C) seasonal hindcast ensemble have been used. These last three models are uncoupled and forced with ~~observations of historical Sea Surface Temperature (SST) fields~~ observed historical SSTs and estimates of ~~SST fields~~ SSTs as they might have been in a counterfactual ~~climate~~ world without anthropogenic climate change. Finally, we used the coupled IPSL-CM6A-LR low-resolution CMIP6 ensemble. The GFDL-CM3 and MPI-ESM models that did not have daily data were not used for the extreme heat analysis. ~~Given that for the FWI~~ For the FWI analysis, which requires daily data of relative humidity (RH), temperature, precipitation and wind speed~~are necessary~~, the list of models used is shortened to CanESM2, CESM1-CAM5, EC-Earth, IPSL-CM6A-LR and weather@home (HadAM3P)~~for that part of the analysis~~.

2.4 Statistical methods

The methods employed in this analysis have been used previously for high and low temperatures (van Oldenborgh et al., 2015; King et al., 2
, extreme precipitation (Schaller et al., 2014; Siswanto et al., 2015; Vautard et al., 2015; Eden et al., 2016; van Oldenborgh et al., 2016; va
, drought (King et al., 2016; Martins et al., 2018; Otto et al., 2018b; Philip et al., 2018c; Uhe et al., 2018) and forest fire weather (Krikken et al., 2019). A paper describing the methods in detail was recently published as Philip et al. (2020).

Changes in the frequency of extreme events are calculated by fitting the data to a statistical distribution. In this study the highest temperature extremes and fire risk-related variables (FWI, MSR) of the fire season are assumed to follow a ~~GEV distribution, while the~~ Generalised Extreme Value (GEV) distribution, which is the distribution that block maxima converge to (Coles, 2001). While our event definition is not exactly block maxima, the GEV fits the data well (see below for more details). The annual mean low precipitation values and lowest monthly precipitation of the fire season are fitted using a Generalized Pareto Distribution (GPD), which describes the exceedance below a low threshold and also allows the specification of a threshold that ensures the PDF is zero for negative precipitation.

The GEV distribution is:

$$P(x) = \exp\left[-\left(1+\xi\frac{x-\mu}{\sigma}\right)^{-1/\xi}\right], \tag{1}$$

where x the variable of interest, e.g., temperature or precipitation~~, $-\infty < \mu < \infty, \sigma > 0, -\infty < \xi < \infty$~~. Here, μ is the location parameter, ~~σ~~ $\sigma > 0$ is the scale parameter, and ξ is the shape parameter. The shape parameter determines the tail behaviour: a negative shape parameter gives an upper bound to the distribution, for $\xi \geq 1$ the tall is so fat that the mean is infinite. The scale parameter corresponds to the variability in the tail.

The GPD gives a 2-parameter description of the tail of the distribution above a threshold, where the low tail of precipitation is first converted to a high tail by multiplying the variable by -1. The GPD is then described by:

$$H(u-x) = 1-\left(1-\frac{\xi x}{\sigma}\right)^{(-1/\xi)}, \tag{2}$$

with x the temperature or precipitation, u the threshold, σ the scale parameter, and ξ the shape parameter determining the tail behaviour. For the low extremes of precipitation, the fit is constrained to have zero probability below zero precipitation ($\xi < 0, \sigma < u\xi$). Calculations ~~have been done~~ were conducted on the lowest 20% and 30% of the data, which ~~gives~~ provide a first-order estimate of the influence of using more or less extreme events. We cannot use ~~fewer points~~ less data as the fits do not converge anymore, and using more than 30% ~~does~~ would not qualify as the 'lower tail'.

Drought, or low precipitation, is particularly difficult to model using the existing extreme value framework (Cooley et al., 2018). While minima can be modelled by multiplying by -1 (Coles, 2001), the applicability of the underlying extreme value theory assumptions still needs to be ~~checked~~validated. In the case of low precipitation, year-on-year autocorrelations are a concern. In southeastern Australia, these serial autocorrelations are approximately $r \approx 0.2$, so although non-zero, do not dominate the drought characteristics. Despite these theoretical limitations, in practice the diagnostic plots show that the Generalised Pareto models ~~explain~~ are able to describe the data reasonably well. In particular, they respect that precipitation is positive-definite. In general this is a difficult problem, and the statistical extremes community ~~are~~ is still developing the solutions necessary for modelling drought events (Naveau et al., 2016).

To calculate a trend in transient data, some parameters in these statistical models are made a function of the 4-yr smoothed global mean surface temperature (GMST) anomaly, T'. This smoothing is the shortest that on the one hand reduces the ENSO component of GMST, which is not externally forced and therefore not relevant, but on the other hand retains as much of the forced variability as possible (Haustein et al., 2019). A longer smoothing time scale would create problems with extrapolation in the highly relevant last few years of the instrumental record. The covariate-dependent function can be inverted and the distribution evaluated for a given year, e.g., a year in the past (with $T' = T'_0$) or the current year ($T' = T'_1$). This ~~gives~~ provides the probabilities for an event at least as extreme as the observed one in these two years~~:~~, p_0 and p_1, or expressed as return periods $\tau_0 = 1/p_0$ and $\tau_1 = 1/p_1$. The change in probability between two such years is called the Probability Ratio (PR): $\mathrm{PR} = p_1/p_0 = \tau_0/\tau_1$.

For extreme temperature we assume that the distribution shifts with GMST: $\mu = \mu_0 + \alpha T'$ or $u = u_0 + \alpha T'$, and $\sigma = \sigma_0$ with α the trend that is fitted together with μ_0 and σ_0. The shape parameter ξ is also assumed constant. For drought and ~~FWI related~~ FWI-related variables we assume the distribution scales with GMST, the scaling approximation (Tebaldi and Arblaster, 2014). In a GEV fit this gives:

$$\begin{aligned} \mu &= \mu_0 \exp(\alpha T'/\mu_0), \\ \sigma &= \sigma_0 \exp(\alpha T'/\mu_0), \end{aligned} \tag{3}$$

and in a GPD fit

$$\begin{aligned} u &= u_0 \exp(\alpha T'/u_0), \\ \sigma &= \sigma_0 \exp(\alpha T'/\mu_0), \end{aligned}$$

with fit parameters σ_0, α and ξ. The threshold u_0 is determined with an iterative procedure and the shape parameter ξ is again assumed constant. The exponential dependence on the covariate is in this case just a convenient way to ensure a positive-definite distribution and has no theoretical justification. For the small trends in this analysis it is similar to a linear dependence.

The validity of the other assumption, that the scale parameter or dispersion parameter are constant, is tested by computation of the significance of deviation of a constant of running (relative) variability plots of the observations and model data (Philip et al., 2020). The analysis of model data is more sensitive to variations of these parameters over time due to the large number of ensemble members but of course assumes the effect of external forcing on the variability is modelled correctly.

For all fits we also estimate 95% uncertainty ranges using a non-parametric bootstrap procedure, in which 1000 derived time series, generated from the original one by selecting random data points with replacement, are analysed in exactly the same way. The 2.5 and 97.5 percentile of the 1000 output parameters (defined as $100i/1001$ with i the rank) are taken as the 95% uncertainty range. For some models with prescribed SSTs or initial conditions ~~the ensemble~~ (in the case of the seasonal forecast ensemble) the ensemble members are found to not be statistically independent, defined here by a correlation coefficient $r > 1/e$ with $e \approx 2.7182$. In those cases the same procedure is followed except that all dependent time series are entered together in the bootstrapped sample, analogous to the method recommended in Coles (2001) to account for temporal dependencies.

When using a GEV to model tail behaviour, note that taking the spatial average of the annual maxima, does not have the same statistical justification as taking the annual maximum of the spatial average (Coles, 2001). Given this, the impact of the

order of operations in the event definition was examined. For ~~heat~~the temperature extremes, we compared the ~~annual time series for the event definition we use, first taking~~ time series where we first take the annual maximum and next the spatial average, to the definition with the order reversed, which can be approximated with a GEV. The Pearson correlation was $r = 0.95$, which is likely due to strong spatial dependence and the concentration of heatwaves at the peak of the seasonal cycle. Therefore, in practice, an approximation with a GEV is not entirely unsuitable for temperature, but caution should be exercised. For the FWI and MSR, the order of operations ~~makes a~~ does make a clear difference. Indeed, we find that the whole distribution is not described well by a GEV for ~~most models. In those cases~~ one climate model used (CanESM2). For that model we take block maxima over ~~5- or 10-ensemble~~ 5-ensemble member blocks, effectively looking only at the most extreme events~~, until the~~ . For this part of the distribution the GEV fit agrees with the data points in the return time plot, as expected from taking block maxima.

We evaluate all climate models on the fitting parameters ~~. For the extremes, we check whether the fit parameters of the distribution from model data agree within uncertainties with those of the observations~~by determining whether the model-derived parameters fall within the uncertainty range of observation-derived parameters. We allow for ~~an overall~~ a mean bias correction, ~~additive for temperature, multiplicative for precipitation and Fire Risk variables~~i.e., we only check the scale and shape parameters σ and ξ. Model biases are accounted for by evaluating the model at the same return time as the value found in the observational analysis. This was found to give better results than applying an additive or multiplicative bias correction to the position parameter μ as it also corrects to first order for biases in the other parameters, especially when the distribution has an upper or lower bound ($\xi < 0$), which is the case in all the cases here.

Finally, observations and all climate models that pass the evaluation test are combined to give a synthesized attribution statement. ~~To obtain a single synthesised attribution statement we first combine the observational results. The spread of the observed estimates stems from the representation uncertainty. This is added to the natural variability as an independent source of uncertainty . In the synthesis figures (Figs~~First, the observations and reanalyses were combined by averaging the best estimate, lower and upper bounds, as the natural variability is strongly correlated as they are largely based on the same observations (except for the long reanalyses). The difference is added as representation uncertainty (white extensions on light blue bars in Figs. S6, S12, S13 and 6. ~~**??, ??, ??** and 6) the solid light blue bars indicate uncertainties due to natural variability, the black outline boxes show natural variability and the dark blue bar represents the consolidated value for observations(reanalyses).~~

~~Next, we combine the results from the model-based analysis, which is the main attribution step. We have two estimates of the uncertainty: the uncertainty range expected from the internal natural variability from the individual fits and the spread of the different model results. We check whether these are compatible by computing the χ^2/dof statistic. If χ^2/dof is greater than one, natural variability alonecannot explain the model spread . We therefore add the model spread to the natural variability, in quadrature as they are independent. In the synthesis figures the model spread is denoted by the white boxes. We next compute a weighted mean by weighing the models by the inverse square of their uncertainties due to natural variabilities, which minimises the uncertainties in the mean.~~ Second, the models were combined by computing a weighted average (using inverse model total variances), as the natural variability in the models, in contrast to the observations, is uncorrelated. However, due to the model spread being larger than expected from variability due to sampling of weather noise alone, a model spread term was added

to each model in addition to the weighted average (white extensions on the light red bars, Figures S5, S6), to account for systematic model errors. This term is defined by requiring that $\chi^2/\mathrm{dof} \leq 1$. The total uncertainty of the models is shown as a bright red bar in these figures. This total uncertainty consists of a weighted mean using the uncorrelated natural variability plus an independent model spread term added to the uncertainty if $\chi^2/\mathrm{dof} > 1$~~.~~, which we do not divide by $\sqrt{N-1}$, i.e., we do not assume that by adding more models to the ensemble the model uncertainty decreases. This procedure is similar to the one employed by Ribes et al. (2020).

Finally, observations and models are synthesised into a single mean and uncertainty range. This can only be done when they appear to be compatible. We show two combinations. The first one is computed by neglecting model uncertainties beyond the model spread. The optimal combination is then the weighted average of models and observations, shown as a magenta bar. However, the total model uncertainty is unknown and can be larger than the model spread. We therefore also show the more conservative estimate of an unweighted average of observations and models ~~. This is indicated in Figs. ?? and ?? by~~ with a white box ~~.~~in the synthesis plots.

3 Extreme heat

3.1 ~~The heat of 2019/20~~

~~Australia started 2019 during an extreme summer that was the country's hottest on record in terms of both seasonal mean and mean maximum temperatures. Both variables broke the previous records set in the 2012/13 season by almost one degree. The summer mean maximum temperature for the 2018/19 season was 2.61 C warmer than the 1961–1990 average. However, many of the temperature records set in early 2019 were eclipsed by the extreme heat during December 2019. This was the hottest month on record in terms of national mean and mean maximum temperature anomalies, respectively at 3.21 and 4.15 C above the 1961–90 December average. The peak of the heat occurred in the week ending the 24th December, which was the country's hottest week on record, at a national mean maximum temperature of 40.5 C. During this week, the highest national mean maximum temperature was recorded on the 17th at 41.9 C, 1 C higher than the previous record, which was set the previous day. In terms of national mean maximum temperatures, eight of the ten hottest days on record occurred in December 2019. While January 2020 was not as extreme as December 2019, it still ranked as the third warmest January on record, with many individual stations in New South Wales observing their highest January temperature on record on the 4th or 5th of the month ().~~ The key takeaways from the attribution analysis of trends in extreme heat are summarized here, while the details are given in the supplementary material, section S1.

~~This record summer occurred, at least in part, in Australia's warmest and driest year on record and directly after the current hottest summer on record (2018/2019 was 1.52 C above the seasonal average). Overall, Australia has warmed by 1 C since 1910, however, most of this warming has occurred since 1950. The frequency of extreme heat events in Australia outnumber extreme cool events by 12:1 (?), and the frequency of heatwaves have also increased since 1950 (?). Increasing trends in heatwave intensity, frequency and duration are projected throughout the 21st Century (?), with a clear link between global warming thresholds and overall heatwave changes (?).~~

3.1 ~~Temporal Event Definition~~

~~For this analysis, we choose an event definition that represents the impacts of extreme heat on the fire risk: the annual (July-June, in order to ensure a continuous summer season) maximum of a~~ Taking advantage of the longer observational record for temperature than for other variables, we analyse the highest 7-day ~~moving average application to daily maximum temperatures, TX7x. Therefore, in this section of the study we aim to answer the question of whether and by how much the probability of a 7-day average maximum temperature at least as high as observed in the study region in 2019 has changed as a result of anthropogenic climate change.~~

3.1 ~~Observational temperature data and methods~~

~~We use a number of datasets developed using independent methodologies to assess observed daily maximum temperatures. The first is the Berkeley Earth climate analysis (?), a gridded dataset derived statistically from available station data. Although maximum daily temperature data is available from 1880 onwards, herewe only use data from 1910 onwards, since the use of Stevenson huts in Australia was only standardised throughout from this time and earlier measurements are likely biased high by several degrees (?). Berkeley Earth uses large decorrelations lengths that are more appropriate for annual than daily data. The next is the Australian Water Availability Project (AWAP) analysis 1910–now, which is constructed by imposing anomalies from station data on a high-resolution climatology. This is augmented by a simple average of a set of quality-controlled Australian Climate Observations Reference Network – Surface Air Temperature (ACORN-SAT) stations (?). These include a large number of coastal stations. The ACORN-SAT daily analysis fields were not yet available at the time of writing.~~

~~We also considered reanalysis data, both long-term reanalyses that are based only on Sea Surface Temperature (SST) and sea-level pressure (SLP), the NOAA Twentieth Century Reanalysis version 3 (20CRv3 ?) and the ECMWF Coupled ReAnalysis of the Twentieth Century 1900-2010 (CERA-20C ?). Finally we used the Japanese ReAnalysis (JRA-55 ?), a reanalysis product from JMA using 4D Variational data assimilation in their TL319 global spectral model spanning 1958-2019 at the time of writing.~~

~~A comparison of the observational analyses reveals striking differences (Fig. ??). The trend in the Berkeley Earth analysis is higher than in the AWAP analysis and high extremes are suppressed, most notably in 1938/39. We looked into this event on 8–14 January 1939 in more detail and ACORN-SAT station data confirms its reality. It even appears in the 20CRv3 reanalysis, which apparently captures the extraordinary circulation that led to the very high temperatures in southeastern Australia that week without assimilating near-surface temperatures. We therefore disregard the Berkeley analysis for the heat extremes in the region of this study. The CERA-20C reanalysis also does not capture this event, which is very relevant for the statistical distribution of heat extremes, so we also do not consider it further.~~

~~The highest 7-day running mean of daily maximum temperature of the July–June year in (top) Berkeley Earth and (bottom) the AWAP analysis. The green line indicates a 10-yr running mean.~~

~~As described in section 2.4, the trend and return period are calculated using the properties of the fit of a Generalized Extreme Value (GEV) distribution, in which the location parameter is a linear model of smoothed Global Mean Surface Temperature~~

(GMST). As the regional event definition has not been selected on the basis of high temperatures we include the year 2019/20 in the fit when available in the datasets. We note that extreme heat GEV distributions have a negative shape parameter; an upper bound exists for the distribution. Hence if the observed 2019/20 event lies above the upper bound of the distribution in 1900, the probability of the event occurring without the GMST trend is zero, and the increase in likelihood due to global warming is formally infinite, although the 95% uncertainty interval usually has a finite lower bound.

3.1 Observational analysis: return time and trend

In the AWAP series the warmest 7-day period so far for the regional index in 2019/20 is 35.9 C, the third-highest value after 1938/39 and 2018/19. It has a return time of about 8 yr (5 … 35 yr). For the reanalyses and model results, which have biases, we use a rounded return time of 10 yr. The GEV fit of the AWAP data gives a return time of 85 yr (35 … ∞ yr) in 1900 (see Fig. **??**, which implies that the probability has increased by a factor of about 11 (3 … ∞) from 1900 to 2019 in this statistical model. The temperature of TX7x has increased by about 1.7 C (0.8 … 2.6 C) in this period. JRA-55 tells a similar story, with a significant temperature increase of 1.5 (1.3-3.4) C extrapolated to 1900–2019.

GEV fit to the AWAP TX7x averaged over the bushfire region. The position parameter μ is assumed linearly dependent on the smoothed GMST and the scale and shape parameters constant. Top: observations (blue symbols), location parameter μ (thick line) and the 6 and 40 yr return values (thin lines). Bottom: return time plot for the climates of 1900 (blue) and 2019 (red), the purple line denotes the 2019/20 event.

3.1 Model evaluation

Left: scale parameter σ (K) in GEV fits of TX7x in observations, reanalyses and climate models. Right: same for the shape parameter ξ.

We consider a set of eight model ensembles that had daily maximum temperatures available to carry out the attribution analysis. To investigate whether the models represent extreme heat well we compare the fit parameters of the tail of the TX7x distribution of the models with those of the observations. In this GEV fit we take the smoothed observed global mean temperature as covariate. The results are shown in Fig. **??**. This shows that most models overestimate the scale parameter σ. This corresponds to the models having too much variability in hot weeks. The same problem was found in the Mediterranean (Kew et al., 2019) and northwestern Europe (**?**). The only exception is the CESM1-CAM5 model, which has too small a scale parameter. This model also has a shape parameter ξ that is incompatible with the fit to observations, all other models agree with the observations in this parameter.

The discrepancy implies that we cannot give quantitative results for the attribution of heat extremes in southeastern Australia, as the heat extremes in the climate models are too different from the observed heat extremes. This affects especially the change in probability, which depends strongly on the variability. For the trend estimates the influence of this shortcoming is smaller. We continue with all models apart from CESM1-CAM5, keeping these limitations in mind.

3.1 ~~Multi-model attribution and synthesis~~

~~We computed trends in the models by either comparing the actual climate 1987–2017 to an estimate of a counterfactual climate of the same period with anthropogenic emissions (weather@home) or by fitting a scaled distribution to the transient data in the same way as for the observational estimates, using the observed smoothed GMST (all other models) as covariate. This revealed two outliers: the ASF20C ensemble has a negative trend over the full 1901-2010 period, so we only use data from 1960 onwards.~~

mean maximum temperatures of the year, averaged over the event domain (Fig. ~~**??** summarises the change in probability and in intensity since 1900 for the 2019 event (observations)and a 10-yr event (the remaining seven models). The observations indicate a 1 to 2 C temperature increase, with a return time of about 10 years. In contrast, the models only simulate about 1 C.~~

~~Synthesis plots of the Probability Ratio PR (left) and change in temperature ΔT (right) between 1900 and 2019 for the observations (blue), models (red). We do not attempt a synthesis as the models disagree too much with the observations.~~

~~Several observational and reanalysis datasets (ACORN stations, CERA-20C) and one model (ASF20C) display what appears to be a non-stationary relationship between TX7x and GMST; as the starting time of a linear regression between them is varied~~ 1), from 1910 ~~onwards, the best-estimate trend increases. For the ACORN stations this is probably due to the varying station coverage, with the trend over the stations active over the early part smaller, maybe more coastal, than over the later part. CERA-20C was excluded for not reproducing the 1929 event. ASF20C is initialised from ocean reanalyses. Due to increasing numbers and quality of observations over the 20th century these change from closer to the model climatology to closer to the real state. This gives time-varying initialisation shocks, which is equivalent to a bias in the trend. Finally in the period before 1950 the global mean temperature was affected as much by volcanic and other natural forcings forcings as it was by greenhouse gases, with possibly different effects from the anthropogenic forcings on circulation. We therefore also show a figure with results from 1950, Fig. **??**, for which more consistent observationsare available, noting that this is a better estimate of the greenhouse-gas driven trend with better observations than the whole period since 1900.~~ (the beginning of standardised temperature observations) to 2019.

~~As Fig. **??** but using only data starting in 1950.~~

~~There are two interpretations of this discrepancy: either the observations are influenced by another driver than anthropogenic climate change that caused the rapid rise in extreme temperatures or the models have problems simulating the response of external forcing on these events and their related processes (or a combination of these two) . As long as it is unknown which of the two explanations is correct we can only quote a lower bound on results, keeping in mind that the true increases could be much higher.~~

~~The Probability Ratios are very roughly ten in the observational datasets, with lower bounds as low as a factor two increase in probability (Fig. **??**). The model results are heavily influenced by the overestimated variability: the high variability in the model, together with the low trends, induces lower probability ratios than in the observations. As there is no overlap between the observed and simulated values we do not attempt to synthesise the results but only quote a lower bound. The spread in the~~

models is compatible with their estimates of natural variability ($\chi^2/dof \approx 1$) so we compute a weighted average. This has an increase in probability between 1900 and 2019 of a factor three with a lower bound of a factor two.

3.1 Conclusions extreme heat

We analysed the highest 7-day mean maximum temperatures of the year averaged over the region south of 29 S between the Great Dividing Range and the sea, the area with most intense bushfires in 2019/20. Observations show that a heatwave as rare as observed in 2019/20 would have been 1 to 2 °C cooler at the beginning of the 20th century . (Fig. S6). Similarly, a heatwave of this intensity would have been less likely by a factor of about 10 in the climate around 1900.

While eight climate models 1900 (Fig. S6). While climate models consistently simulate increasing temperature trends over this time period, they all have some limitations for simulating heat extremes: the variability is in general of 7-day mean maximum temperature is generally too high and the trend in these heat extremes long-term trend is only 1 °C . (Fig. S5 and Fig. S6). We can therefore only conclude that anthropogenic climate change has made a hot week like the one in December 2019 more likely by at least a factor of two. Given the larger trend in observations in the models we suspect that climate models underestimate the trend due to climate change. Coupled with the high variability of the models, the increase in the likelihood of such an event to occur is likely much higher than the models simulate.

4 Meteorological drought

3.1 Temporal Event Definition

, but cannot give a best estimate or upper bound due to the model deficiencies limiting our confidence in the exact magnitude of the anthropogenic influence.

Next we analyse meteorological drought, that is, low precipitation. The formulation of the Fire Weather Index only considers precipitation over the last 52 days, as a proxy for this we also analyse the driest month in the fire season September–December. December 2019 was one of the driest months on record in our study region in southeastern Australia since 1900 (third in GPCC, ninth in AWAP). Using monthly data means we can utilise the models described above, thus sampling model spread as well as possible.

The January–December annual mean 2019 was the driest year on record since 1900 (). This was also the case in our study region in southeastern Australia, which could play a role in the bushfire risk that is not parameterised by the FWI. The two previous years had also been very dry, but it is unclear whether this still affects the 2019/20 bushfires. We therefore also analyse annual mean drought but not multi-year drought.

3.1 Observational precipitation data and methods

We considered three observational datasets of monthly precipitation: GPCC v18 1900–2018 (?) extended with the monitoring analysis (?) up to November 2019 and the first guess analysis (?) up to January 2020, CRU TS 4.03 1901–2017 (?) and AWAP

1900–January 2020 (). As the distributions of annual mean precipitation and the driest month in the fire season are both not described well by a Gaussian we use a GPD fit to the lowest 20% or 30% for the observations, demanding that it has a lower bound ($\xi < 0$) that is larger than zero ($\sigma < -\xi u$) so that there is no probability for negative precipitation.

3.1 Observational analysis: return time and trend

For the annual mean low precipitation analysis the fit for AWAP data using the lowest 20% is shown in Fig. **??**. The year 2019 is not included in the fit. This fit shows a significant trend towards more dry extremes over the period 1900-2018. The return time of 16 yr (3 … 550 yr) is the lowest in the observational datasets. The fit should be independent of the threshold, but this is not the case: whereas the lowest 20% show a significant downward trend, the GPD fit to the lowest 30% has an upward trend that is not significant at $p < 0.05$ (two-sided) in the AWAP dataset (Fig. **??**, right). The lowest 10% does not contain enough data to fit a GPD. We report both the 20% and 30% choices in the following.

GPD fit to the AWAP estimate of annual mean precipitation in the bushfire region. The position and scale parameters depend exponentially on the observed smoothed global mean surface temperature such that their ratio is constant. The scale parameter is forced to be negative and the cut-off zero or higher. Left: using the lowest 20%. Right: using the lowest 30%. Top: observations (blue symbols), location parameter μ (thick line) and the 6 and 40 yr return values (thin lines). Bottom: return time plot for the climates of 1900 (blue) and 2019 (red), the purple line denotes the 2019/20 event.

The return time of the low 2019 precipitation depends strongly on the observational dataset and the cut-off in the GPD fit and ranges from 25 yr (3 … 4000 yr) in GPCC 30% to infinity in the AWAP fits with large uncertainty ranges starting at 3 yr, with GPCC 20% intermediate at 120 yr (3 … 3000 yr). The uncertainty ranges are in fact more similar than the best fit values. Also given that it was the lowest value in 120 years we evaluate the models at the rounded return time of 100 yr.

We also fit a GPD to the lowest 20% and 30% of monthly precipitation amounts in the fire season September–February. For some of the models we only had the driest month per season and the threshold is taken over the driest month in all ensemble members. These extremes are more difficult to fit because the values approach the lower boundary of zero. In fact, in some bootstrapped time series no initial conditions for the fit routine that satisfy all constraints could be found. The result is that the uncertainty range is too small for some fits and does not encompass the best fit.

The driest month in 2019/20 was December 2019. The return times obtained from the fits again vary widely, from 75 yr (15 … 200 yr) to 800 yr (10 250 yr), both for the GPCC analysis for the 20% and 30% thresholds. For the models we use a return time of 100 yr.

3.1 Model evaluation

We have data for the annual mean drought and driest month of the fire season for ten climate model ensembles. The ASF20C model only has 4-month runs starting four times per year and therefore cannot provide annual mean precipitation nor the driest month in the fire season and is not included here.

The dispersion parameter σ/μ (left) and shape parameter ξ (right) of GPD fits to the low tail of the annual mean precipitation distribution in observations (blue, lowest 20% and 30%) and models (red, lowest 20%).

Fig. ?? shows that the statistical description of the low tail of annual mean precipitation of all models agrees with the same quantities in the observations within the (large) uncertainties due to natural variability.

As Fig. ?? but for the driest month in the fire season September–February. The bootstrapped uncertainty intervals are sometimes underestimated due to fitting problems.

Fig. ?? shows that also for the driest month in the fire season all models have statistical descriptions of the low tail of the distribution that agree with the description of the observed tail within the large uncertainties of the various estimates of the observed climate .

3.1 Multi-model attribution and synthesis

PR (left) and ΔP (%) (right) for annual mean low precipitation. The purple bar indicates the weighted average under the assumption that the model spread is equal to the model uncertainty, the white box around this purple bar gives equal weight to the observations and models.

Fig. ?? shows the change in probability and intensity of annual mean drought averaged over the bushfire region in southeastern Australia. The observations show a positive probability ratio PR and smaller intensities of low precipitation events, which implies a shift towards a larger probability for drought over the last 120 years. However, the models show no trend , so we cannot attribute these shifts to anthropogenic climate change. The observed trends can be due to natural variability (note that the 95% uncertainties encompass no change and these ignore the year-to-year autocorrelations, reasons for the lag-1 autocorrelation is borderline significantly different from zero, $\alpha_1 \approx 0.2$). Another possibility is that they are due to other drivers not included in this analysis. Finally, apparent model deficiencies in simulating trends and variability in extreme temperatures are not fully understood. In section S3 we show that the temperature variability explained by the Indian Ocean Dipole (IOD) and Southern Annual Mode (SAM) is too small to explain these mismatches as problems in the model representation of these modes of variability. The literature suggests that shortcomings in the coupling to land and vegetation (e.g., Fischer et al., 2007; Kala et al., 2016) and in parametrisation of irrigation (e.g., Thiery et al., 2017; Mathur and AchutaRao, 2019) in the exchange of heat and moisture with the atmosphere, and also in the representation of the boundary layers (e.g., Miralles et al., 2014) are more likely to be the cause of the problems. Given the larger trend in observations than in the models we suspect that climate models underestimate the trend in extreme temperatures due to climate change, although in principle the difference could again also be due to shortcomings in the climate models. Note that the large natural variability can hide these shortcomings in the model evaluation in section ??.

Following ? we investigate whether the lack of trend in the models is just due to high natural variability masking the trend by repeating the analysis using data up to 2100 for all models that also have future data (CanESM2, CESM1-CAM5, CSIRO Mk3.6.0, EC-Earth, GFDL-CM3, GFDL-ESM2M, MPI-ESM), using the model ensemble-averaged GMST as covariate. The reduced natural variability reveals a larger model uncertainty, but taking this into account the model trend is between −7% and +7%, showing no systematic trend towards more dry extremes (not shown)a non-climatic driver that affects the trend in observations. The combination of a weaker trend and higher variability in models compared to observations yields an increase in the likelihood of such an event that is much higher in observations than in models.

It should be noted that some of the models show large trends towards more drought in mean precipitation . What we find hereis that 1 in 100 yr dry extremes do not follow this trend but stay relatively constant.

4 Meteorological drought

PR (left) and ΔP (%) (right) for the driest month in September–February. The purple bar indicates the weighted average under the assumption that the model spread is equal to the model uncertainty, the white box around this purple bar gives equal weight to the observations and models. For most observational datasets and some models the uncertainty range is underestimated due to problems fitting the data, this is taken care of in the averages by increasing the representation error and model spread terms (white boxes).

The summary figures for the driest month of the fire season The key takeaways from the attribution analysis of trends in low precipitation are summarized here, while the details are given in the supplementary material, section S2. The conclusions below are shown in Fig. **??**. Although the fits are not very good, both observations and models indicate a small, non-significant increase in precipitation, which is equivalent to a decrease in probability to observe as dry a month as December 2019 (PR $<$ 1).Due to the fact that the uncertainties in the PR and ΔP encompass zero, there is no attributable trend in the occurrence of very dry months in the fire seasonS12 for annual mean drought and Fig. S13 for the driest month of the year.

4.1 Conclusions meteorological drought

Observations show non-significant trends towards more dry extremes like the record 2019 annual mean and a non-significant trend towards fewer dry months like December 2019 in the fire season . (Fig. S12 and Fig. S13). All ten climate models we considered simulate the statistical properties of the observations well . (Fig. S10 and Fig. S11). Collectively they show no trend in dry extremes of annual mean precipitation nor in the driest month of the fire season (September–February). We conclude that there is no evidence for an attributable trend in either kind of dry meteorological drought extremes like the ones observed in 2019.

5 Fire risk indices

5.1 The fire weather of 2019/20

As discussed in the introduction, the fire risk as parametrised by the definitions below were described by fire weather indices was extreme in the study area domain in the 2019/20 fire season. This was reflected by disastrous fires during the season. The region The domain was chosen to encompass these fires and therefore the 2019/20 event cannot be included in the fitsstatistical analysis.

5.2 Temporal Event Definition

~~For this analysis we~~ We choose two event definitions in order to represent two important aspects of the event, namely the intensity and the duration. For ~~the former~~intensity, we first select the maximum FWI of a 7-day moving average over the fire season (September–February) for every grid point over the study region, after which we compute the spatial average~~. This event definition will tell us more on changes in intensity of the bushfire season, and is hereafter labeled as~~ , hereafter FWI7x-SM (seasonal maximum). ~~For the latter we compute~~ The 7-day time scale was chosen based on a good correlation with the area burnt (see Fig. 2) and good correspondence with area burnt in other forest fire attributions studies (Krikken et al., 2019).

For duration, we consider the monthly severity rating (MSR). The MSR is the monthly averaged value of the daily severity rating (DSR), which in turn is a transformation of the FWI ($\mathrm{DSR} = 0.0272\mathrm{FWI}^{1.71}$). The DSR reflects better how difficult a fire is to suppress, while the MSR is a common metric for assessing fire weather on monthly time scales (Van Wagner, 1970). For this ~~event~~study, we select the maximum value of the MSR ~~of~~ during the fire season over the study area (MSR-SM). In contrast to the FWI7x-SM, we first apply a spatial average of the study area and then select the maximum value per fire season. This event definition ~~provides information~~ focuses more on changes in extreme fire weather for ~~both~~ longer time scales and larger ~~areas.~~ integrated areas than FWI7x-SM. Note that neither of the two event definitions includes ignition sources or small-scale meteorological factors such as pyrocumunimbus development that could enhance the fires.

5.3 Observational analysis: return time and trend

For the observational analysis we use the fifth generation European Centre for Medium-Range Weather Forecasts (ECMWF) Atmospheric Reanalysis (ERA5~~reanalysis~~) dataset 1979–January 2020 (Hersbach et al., 2019). This reanalysis dataset is heavily constrained by observations, thus providing one of the best estimates of the actual state of the atmosphere for all the variables needed to compute the FWI over the study area. Other reanalyses did not yet include the full 2019/20 event at the time of the analysis.

Fig. 3 shows the time series of the highest 7-day-mean FWI averaged over the study area. Both for the FWI7x-SM and MSR-SM the event is the highest over the 1979–2020 time period. Note that for the MSR-SM, the value is considerably more extreme than for the FWI7x-SM. The GEV-fits (Fig. 3, right) illustrate this further, with return times in excess of 1000 years.

A fit allowing for scaling with the smoothed GMST gives a significant trend in the ~~highest 7-day mean FWI, averaged over the study area~~ FWI7x-SM (Fig. 4). This fit gives a return time ~~of the maximum in the~~ for the 2019/20 fire season of about 31 yr (4 to 500 yr) in the current climate and more than 800 yr extrapolated to the climate of 1900. This corresponds to an infinite PR, with a lower bound of four.

~~For the~~ The return time for MSR-SM is undefined and is thus estimated to be 100 years. For the climate model analysis we ~~will use a return time~~ thus use return times of 31 years for the FWI7x-SM ~~. Because the return time for MSR-SM is undefined, we select a return time of~~ and 100 years for ~~the models analysis~~MSR-SM to determine the event thresholds in individual climate models.

5.4 Model evaluation

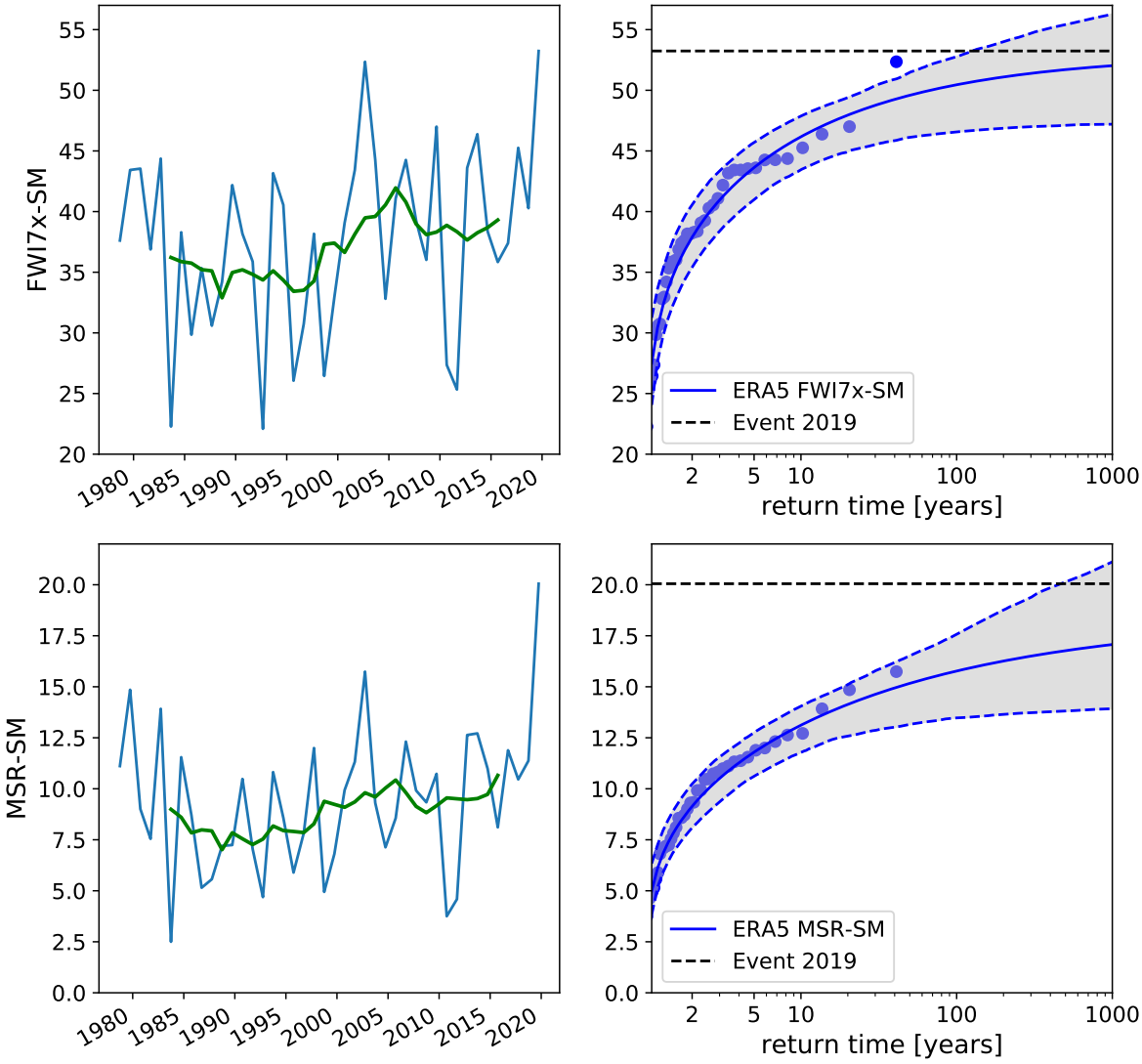

Figure 3. Left: time series with 10-yr running mean of the area-average of the highest 7-day mean Fire Weather Index in September–February (top) and ~~MSR September-February~~ Monthly Severity Rating September–February maximum (bottom). Right: stationary GEV fit to these data, the dots represent the ordered years.

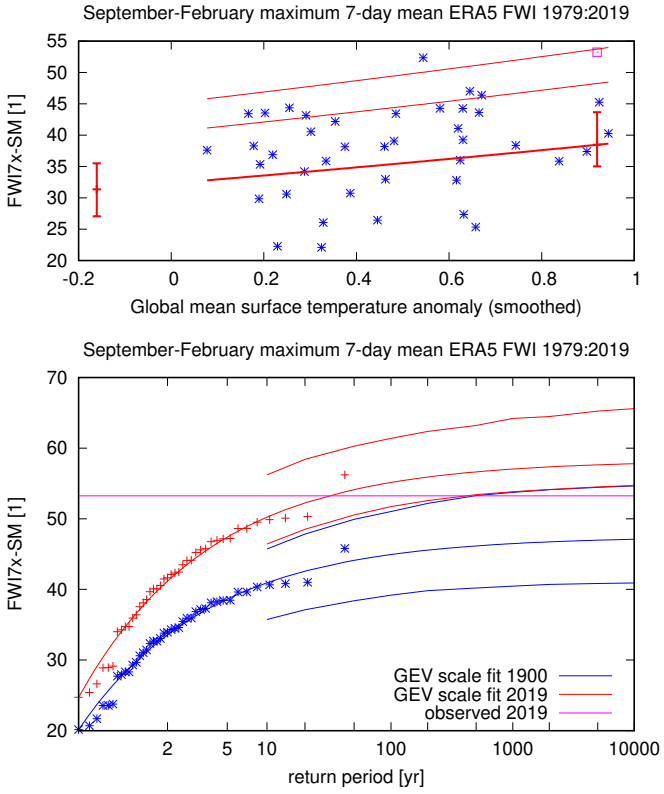

Figure 4. Fit of a GEV that scales with the smoothed GSMT (Eqs 1,3) of the highest 7-day mean FWI computed from the ERA5 reanalysis, averaged over the index region. Top: observations (blue symbols), location parameter μ (thick line and uncertainties in 1900 (extrapolated) and 2019/20) and the 6 and 40 yr return values (thin lines). The purple square denotes the 2019/20 value, which is not included in the fit. Bottom: return time plot with fits for the climates of 1900 (blue lines with 95% confidence interval) and 2019 (red lines), the purple line denotes the 2019/20 event. The observations are plotted twice, shifted down to the climate of 1900 (blue stars) and up to the climate of 2019 (red pluses) using the fitted dependence on smoothed global mean temperature so that they can be compared with the fits for those years.

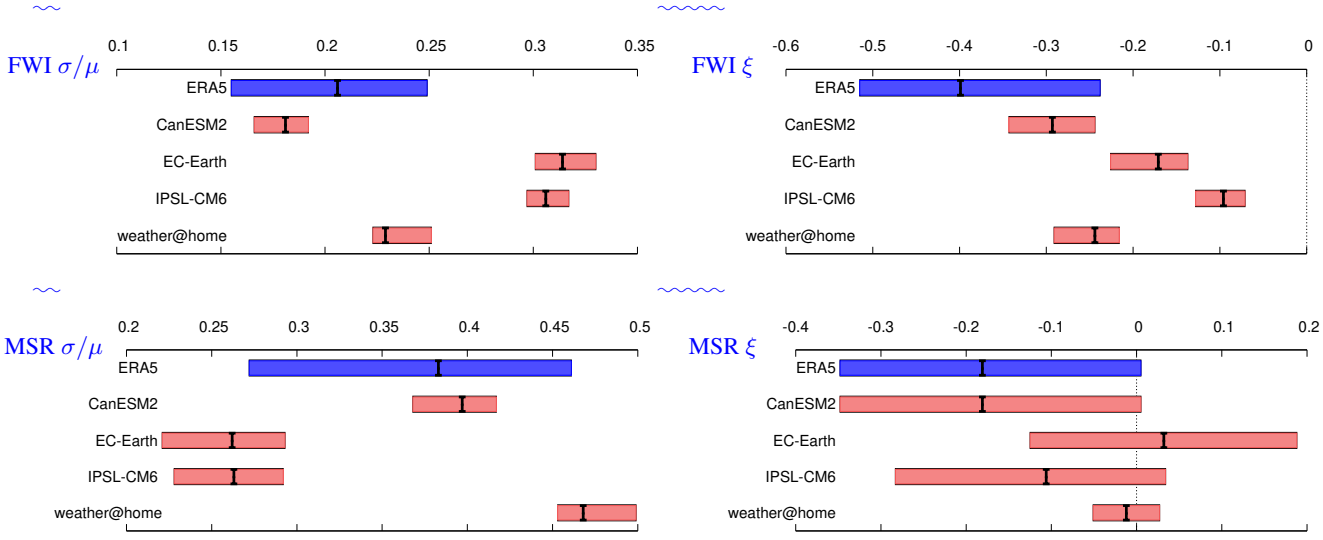

Figure 5. Model verification for FWI (top) MSR (bottom). The left figures show the dispersion parameter σ/μ and the right figures the shape parameter ξ.

~~For the model analysis we~~ We use four climate models with large ensembles, leaving out CESM1-CAM5 because of its failure to represent heat extremes (see section 3). This is fewer than for the drought and heat analysis, because the FWI requires four daily input variables, which are not available for all models. In contrast to the heat extremes and drought analyses, the models use as covariate the model GMST, and take as reference climates, where the years at which it is evaluated is taken from the 1.1 °C temperature increase for the present-day climate and the 2 °C increase for the future reference climate and not 2019 and 2060. As the fits are invariant under a scaling of the covariate this does not make much difference.

First the models are evaluated on how well they represent the extremes of FWI7x-SM and MSR-SM. This is quantified by the dispersion parameter σ/μ and shape parameter ξ ~~,~~ of the GEV fit for the present-day climate. We do not check the position parameter μ, assuming a multiplicative bias correction can be applied.

Fig. 5 gives an overview of these parameters. Preferably, we would like the parameters to lie within the observational uncertainty ~~(~~from ERA5~~)~~. For the dispersion parameter CanESM2 and weather@home fall within the observational uncertainty of the FWI. The other two models (EC-Earth and IPSL CM6) show too much variability relative to the mean. The same holds for the shape parameter. This implies that it is difficult to draw strong conclusions from the model data, given that they do not accurately represent the ~~extreme fire weather events~~extremes of FWI7x-SM. In particular, the models with too much variability will underestimate the probability ratios. We continue with all four models~~keeping~~ , but keep these problems in mind.

The MSR is simulated better: all model dispersion and shape parameters lie within the large observational uncertainties, although they largely disagree with one another ~~in~~ on the dispersion parameter.

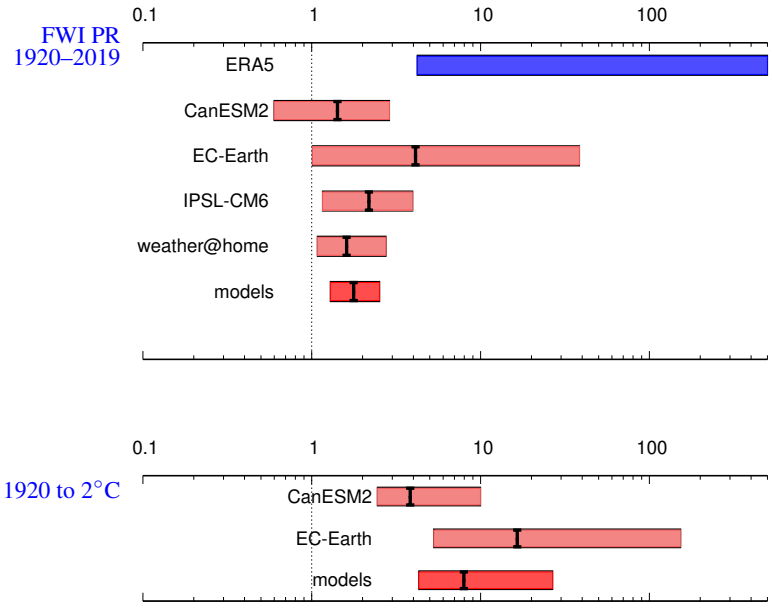

Figure 6. Top: PR for a FWI as high as observed in 2019/20 or higher, (top) from 1920/21 to 2019/20 and (bottom) from 1900 to a climate globally 2 °C warmer than ~~late~~ 1920. The last row is the weighted average of all models, the spread of which is consistent with only natural variability. Bottom: same for a 2 °C climate (GMST change from late 19th century).

5.5 Multi-model attribution and synthesis

The model results are summarized by their ~~probability ratio~~PR, i.e., how more or less likely such an event will be for present or future climate, relative to the early 20th century.

Figs. 6 and 7 show the change in probability for both the FWI7x-SM, and the MSR-SM from 1920 to 2019 (denoting the 2019/20 fire season). For the FWI7x-SM, all models agree on an increased ~~risk for this event for~~ probability for such an event in the present climate relative to the early 20th century, although the trend is not significant at $p < 0.05$ two-sided for one of the models, CanESM2. As the spread of the models is compatible with natural variability ($\chi^2/\mathrm{dof} < 1$) we take a weighted average ~~.~~ across the models to synthesize them (Fig. 6). This shows that such an event has become about 80% more likely in the models, with a lower bound of 30%. Note that all models severely underestimate the increased risk compared to ERA5, which has a lower bound PR of a factor four relative to 1920 (extrapolated), above the upper end of the model average.

For a future climate of 2 °C warming above pre-industrial we find that such events become about eight times more likely in the models, with a lower bound of about four times more likely. Note that the estimate of future climate is only based on two climate models, CanESM2 and EC-Earth, due to the absence of future data for the others.

For the MSR-SM ~~we find on average~~ the models on average show about a doubling of probability for the present climate relative to the early 20th century ~~climate an increased risk of about two times more likely.~~(Fig. 7). However, this trend is not

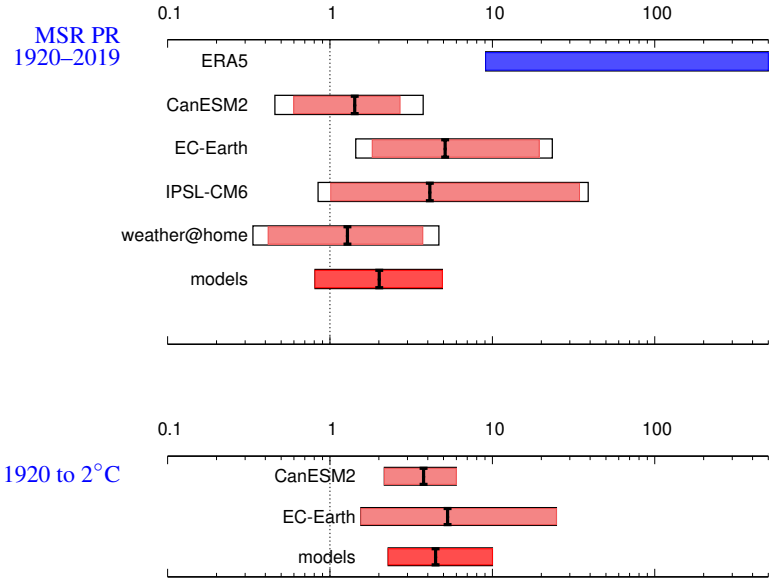

Figure 7. As Fig. 6 but for the Monthly Severity Rating (MSR).

significant as the lower bound is 0.8, i.e., a decreased ~~risk~~ probability is also possible within the two-sided 95% uncertainty range. ~~For~~ In the fit to the ERA5 data we include 2019, as otherwise the probability of the event occurring in the current climate would be zero, contrary to the fact that it did occur. This fit shows much higher probability ratios, with a lower bound of a factor nine. As there is no overlap with the model results we cannot combine the model and observational results, but only give a conservative lower bound as an observations-model synthesis result. For a future climate relative to the early 20th century climate ~~we find an increased risk~~ the models show an increase in probability of about four times~~more likely~~ , with a lower bound of two. ~~Again, the fit to ERA5 data (including 2019) shows much higher probability ratios, with no overlap with the model results.~~

5.6 Interpretation

The underestimation of the observed trend in fire weather indices in all models and the tendency for too much variability in some models is reminiscent of the extreme ~~heat results in section 3 .~~ temperature results in sections 3 and S1.

In order to better understand which input variables cause the ~~increased FWI, we select~~ long-term increase in FWI7x-SM and thus the contribution to the 2019/20 FWI7x-SM value, we study the input variables ~~during~~ to FWI7x-SM separately for each model as well as observations. For precipitation we ~~select~~ use the cumulative precipitation (90 days) prior to ~~the maximum value. By comparing these values for the~~ each FWI7x-SM value. We calculate the change from the early 20th century ~~climate and present day we get the change in the input parameters during high FWI events. To analyse their individual impact on the FWI,~~ to present day in each input variable to estimate its long-term change, which we then subtract ~~these changes of the input~~

parameters calculated from model data to the ERA5 from that variable's observed value in 2019data, and recompute the FWI for the adjusted /20. We then recalculate FWI7x-SM, but using each detrended individual input variables in turn. Each of these newly calculated FWI7x-SM values thus illustrates the influence of the long-term trend in a particular input variable onto the observed 2019event/20 FWI7x-SM value. This procedure is applied to models and ERA5. In the models, the ensemble mean change is used to estimate an individual variable's long-term trend, whereas in ERA5 a regression of each variable onto GMST is used to estimate its early 20th century value. The results of this analysis for the 2019/20 FWI7x-SM value are shown in Fig. 9.

First it should be noted that the The sum of the individual contributions matches with the total effect , so the individual components add linearly . Second, the contributions from individual input variables to the 2019/20 FWI7x-SM anomaly match the effect of changing all variables at the same time, so can be considered linearly additive Fig. 9.. The underestimation of the heat trends in these extreme temperature trends in the climate models carries over into this analysis, so the temperature bars are underestimated. Even with such that the temperature contribution to the observed 2019/20 value is underestimated. Despite this underestimation, for temperature emerges as the most important variable in EC-Earth and weather@hometemperature is most important, as it explains roughly half of the increase in FWI. For IPSL, the simulated temperature increase explains about a third of the FWI7x-SM increase, together with wind and RH. CanESM2 behaves differently, where it is mainly the decrease of RH that explains the higher FWIFWI7x-SM. Most, but not all models analysed here therefore derive the increase in FWI to a large extent FWI7x-SM largely from the increase in temperature of heat extremes. For extremes.

In ERA5 the increase in temperature also appears to be most important in explaining the increased FWI, and to a lesser extent a decrease of the most important explanatory variable, followed by a decrease in RH and precipitation.

These results are in agreement with the findings from the heat attribution (section 3), given thatwe find an increase in temperature during high FWI events for all models. The underestimation of these models of the trends in heat extremes is therefore part of the explanation that all models underestimate the increase in FWI compared to the observationsAs we did not find a significant trend in precipitation over longer time periods, we hypothesize this trend to be due to natural variability over the short 1979–2018 period in ERA5. We explicitly verified that the dependence of the FWI7x-SM on temperature is almost linear in a range of ± 5 K around the reanalysis value (not shown). Further, volumetric soil water (Fig. 8) at multiple soil layers from ERA5 suggests that, despite the soil already being very dry in 2018 and into 2019, the 2019/20 austral spring-summer drought caused a further drying of the soil in the study area. This suggests that the late 2019 drought and high temperatures did indeed cause an additional increase in fire risk over preceding years.

.

5.7 Conclusions fire risk indices

The observations of the Fire Weather Index show FWI7x-SM as computed from the ERA5 reanalysis as an approximation to the real world shows that the 2019/20 values were exceptional. They have a significant trend towards higher fire weather risk since 1979. Compared with the climate of 1900, the probability of Fire Weather Index a FWI7x-SM as high as in 2019/20 has

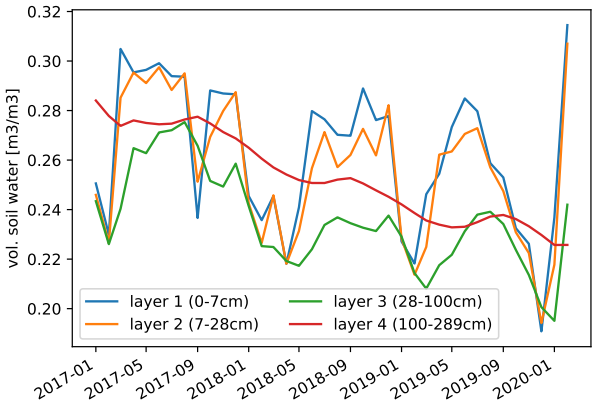

Figure 8. ERA5 volumetric soil water from multiple levels. The data represents the spatial average over the study area.

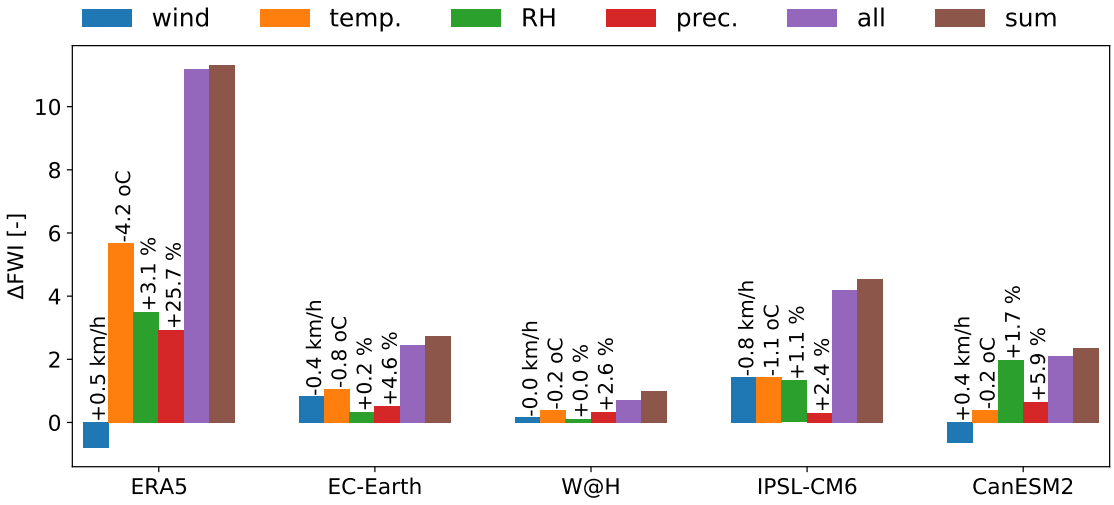

Figure 9. Sensitivity analysis ~~for~~ of the ~~FWI on the~~ FWI7x-SM to changes in individual ~~contribution of~~ contributions from relative humidity (RH, wind, temperature and precipitation~~for all models used~~. The relative increases or decreases for the individual variables of the climate models are based on the average change in input variables ~~during the seasonal maximum FWI7x~~ between present day and the early 20th century climate ~~. These~~ (values ~~are plotted~~ above ~~the~~ bars). For ERA5 the changes are based on a linear regression of the ~~input variables during FWI7x-SM with~~ respective variable onto GMST for the years 1979 to ~~2018.~~ 2018, and then extrapolated to the early 20th century. These changes are subtracted from the 2019 ERA5 data, after which the FWI is recomputed, where ΔFWI is the original FWI minus the altered FWI. In the 'all' experiment all input ~~parameters~~ variables are changed simultaneously. 'Sum' is the sum of all the individual changes in FWI.

increased by more than a factor of four. For the ~~Monthly Severity Rating~~ MSR-SM the probability has increased by more than a factor of nine.

The four climate models investigated show that the probability of a Fire Weather Index this high has increased by at least 30% since 1900 as a result of anthropogenic climate change. As the trend in extreme ~~heat is one of the main factors~~ temperature is a driving factor behind this increase and the climate models underestimate the observed trend in ~~heat, the real increase~~ extreme temperature, the attributable increase in fire risk could be much higher. This is also reflected by a larger trend in the ~~Fire Weather Index in the observations.~~

~~The Monthly Severity Index~~ FWI7x-SM in the reanalysis compared to models. The MSR-SM increased by a factor of two in the models ~~, compared with~~ since 1900, ~~but this~~ although this increase is not significantly different from ~~no change. Again, the real~~ zero. As with FWI7x-SM , the attributable increase is likely ~~much higher~~ higher due to the model underestimation of temperature trends and overestimation of variability in TX7x.

Projected into the future, the models ~~simulate that a Fire Weather Index at the~~ project that a FWI7x-SM as high as 2019/20 ~~level would be~~ would become at least four times more likely with a 2 °C temperature rise, compared with 1900. Due to the model limitations described above this ~~is likely an underestimate.~~ could also be an underestimate.

6 Other drivers

~~There are known associations between large-scale climate drivers, such as El Niño—Southern Oscillation (ENSO), the Indian Ocean Dipole (IOD) and the Southern Annular Mode (SAM), and fire risk (e.g., **??**Harris and Lucas, 2019; **?**). These drivers of interannual variability can dominate the risk of fire weather over the trend in individual years (Harris and Lucas, 2019).~~

6.1 ~~ENSO~~

~~ENSO variations are linked to Australia's climate variability, with generally warm and dry conditions in eastern Australia during El Niño, although the signal is weaker on the east coast. ENSO was considered neutral during 2019/20, however, the western Pacific was anomalously warm and the Niño4 index indicated El Niño conditions of the Central Pacific 'flavour' (**?**) with the relative Niño4 index in which the climate change signal is removed (**?**) around +0.6 C during the 2019/20 fire season. The index that connects best with global teleconnections, relative Niño3.4 anomalies, was neutral during the period. However, the atmospheric state was also typical for weak El Niño conditions with the Southern Oscillation Index (SOI) of the National Centers for Environmental Prediction (NCEP) at around −0.6 until December 2019, perhaps encouraging an enhancement of the IOD via atmospheric teleconnections (**?**).~~

6.1 ~~Indian Ocean Dipole~~

~~The IOD is an interaction between the ocean and atmosphere in the tropical Indian Ocean basin with climatic influences around this basin (**?**). In general, IOD events develop in the Southern Hemisphere winter through spring, and break down with the start of the Indonesian monsoon in early summer. It is thus not an important driver through summer. In the positive phase, colder~~

than normal sea surface temperatures are observed in the eastern Indian Ocean (around Sumatra and Java). Positive IOD events are typically associated with below average winter-spring rainfall in Southern Australia and warmer than average conditions (**?**). As a result, IOD positive phases are associated with severe bushfire conditions (Harris and Lucas, 2019; **?**).

In 2019, an unusually strong positive IOD event was observed, which, together with the Southern Annular Mode, was argued to be primarily responsible for the precipitation deficit over South-Eastern Australia ((**?**)). This event started to emerge in June but matured and strengthened during early austral Spring. The late onset of the monsoon off Sumatra also led to the unusual persistence of the IOD into early summer in 2019. Variations in the IOD (as measured by the Dipole Model Index, DMI) explain only a small fraction of variance in observed temperatures in SON. In particular, the correlation with the AWAP TX7x index defined in section 3 is only $r = 0.22$. The correlation with the AWAP precipitation in July–December is much higher, $r = -0.4$.

This does include some double-counting in the statistical relation: as the IOD is often partially forced by ENSO, a fraction of these correlations are in fact ENSO teleconnections (although the influence was minor in 2019). When the influence of ENSO teleconnections, expressed as the regression on the relative Niño3.4 index, is linearly removed from the DMI these correlations become much lower, with no significant connection with TX7x and a correlation of $r = -0.22$ with July–December rainfall (Fig. **??**). However, even with this low correlation, the very high positive IOD conditions observed in July-December 2019 account for approximately one third of the July-December low rainfall, see Fig. **??**. We chose this half year as it precedes the fire season September–February and therefore represents some of the drought preconditioning of the fire weather risk in this season. As the Niño3.4 index was neutral it did not contribute to the drought in the second half of 2019, although as mentioned above western Pacific SST and the atmospheric circulation did indicate a weak El Niño.

Scatterplot of AWAP precipitation averaged over the bushfire region in southeastern Australia preceding the fire season, July–December as a function of the DMI index with the monthly linear regression on the relative Niño3.4 index subtracted.

6.1 Southern Annular Mode and stratospheric preconditioning

The Southern Annular Mode (SAM) is an important mode of climate variability in the Southern Hemisphere related to variations in the large-scale atmospheric circulation. The positive phase of the SAM is associated with a stronger and more contracted stratospheric polar vortex and a stronger and more poleward located mid-latitude storm track. The impact of the SAM on the Australian climate variability is seasonally dependent and opposite precipitation responses are found in different regions of the continent. Based on ERA-Interim reanalysis data, a strong negative subtropical precipitation response during spring and summer in southeast Australia has been found for the negative phase of the SAM (**?**). During most of the second half of 2019 (July–December) the SAM phase was negative, with strong negative index values in November 2019. This negative phase of the SAM during 2019 has contributed roughly another one third to the extreme drought conditions in southeast Australia from July to December (Fig. **??**). We did not find a significant correlation with our measure of heat waves, TX7x, in agreement with **?**.

Scatterplot of AWAP precipitation averaged over the bushfire region in southeastern Australia preceding the fire season, July–December as a function of the SAM index.

The ~~strong SAM excursion of 2019 was very well predicted. One cause was a Sudden Stratospheric Warming (SSW) event, where the winter stratospheric vortex over Antarctica breaks down and the stratosphere warms rapidly. These are rare events, with only two major events recorded, in 2002 and 2019. In 2019, the negative phase of the SAM from October onwards has been preconditioned by the preceding SSW event through a downward coupling of the weakened polar vortex to tropospheric levels as highlighted by **?**. SSW events are thus associated with warm and dry conditions over eastern Australia (**?**).~~

~~Another interconnected cause of the record SAM state was the strong positive ozone anomaly in September, associated with a relatively warm polar stratosphere and an exceptionally weak ozone hole season (). This was followed by a period with a negative phase of the SAM from October onwards which in line with the ozone-SAM correlations found by **???**.~~

6.1 ~~Conclusions other drivers~~

~~The~~ attribution statements presented in this paper are for events defined as meeting or exceeding the threshold set by the 2019/20 fire season and thus assessing the overall effect of human-induced climate change on these ~~kind~~ kinds of events. In individual years, however, large scale climate system drivers can have a higher influence on fire risk than the trend. A detailed analysis of the influence of ENSO, the IOD and SAM is presented in section S3.

Besides the influence of anthropogenic climate change, the particular 2019 event was made much more severe by a record positive excursion of the Indian Ocean Dipole and a very strong negative anomaly of the Southern Annular Mode, which ~~together explain more than half of the amplitude of the meteorological drought (precipitation deficit)~~likely contributed substantially to the precipitation deficit. We did not find a connection of either mode to heat extremes. More quantitative estimates will require further analysis and dedicated model experiments, as the linearity of the relationship between these indices and the regional climate is not verifiable from observations alone.

7 Vulnerability and exposure

At least 19.4 million hectares of land have ~~burned~~ burnt as a result of the Black Summer Bush Fires of 2019/20 (CDP, 2020). This has resulted in 34 direct deaths and the destruction of 5,900 residential and public structures (IFRC, 2020). Nearly 80% of Australians reported being impacted in some way by the bushfires (The Conversation, 17 February 2020). In Sydney, Canberra and a number of other cities, towns and communities air quality levels reached hazardous levels (NY Times, 3 January 2020). Over 65,000 people registered on Australian Red Cross' reunification site to look for friends and family, or to let loved ones know that they were ~~all right~~ alright (Australian Red Cross, 2020). It is estimated that over 1.5 billion animals have died nationally (Reliefweb Australia: bushfires, 2020). These impacts are not only hazard-related but also related to various vulnerability and exposure factors that each play a role in increasing or decreasing risk and impacts. Vulnerability is defined as 'The propensity or predisposition to be adversely affected. Vulnerability encompasses a variety of concepts and elements including sensitivity or susceptibility to harm and lack of capacity to cope and adapt' (Agard et al., 2014). It can also be defined as 'the diminished capacity of an individual or group to anticipate, cope with, resist and recover from the impact of a natural or man-made hazard' (IFRC, 1 March 2020). Exposure is defined as 'The presence of people, livelihoods, species or ecosystems,

environmental functions, services, and resources, infrastructure, or economic, social, or cultural assets in places and settings that could be adversely affected' (Agard et al., 2014).

Bushfires have been a part of the Australian landscape for millions of years, and are an ever-present risk for people living in rural and peri-urban areas surrounded by vegetation/bush/grasslands. ~~Significant bushfires in the recent past include: Black Saturday in 2009 where 450, 000 hectares burned and 173 people died (); the~~ In recent decades, significant bushfires occurred in 1974/75, 1983, 2002/03~~bushfire season where 38 million hectares burned and seven people died (?); the Ash Wednesday bushfires in 1983 where 400, 000 hectares burned and 75 people died (); and the 1974~~, and 2009, some of them including grass fires, which can have different drivers to forest fires like 2019/~~75 bushfires where 117 million hectares burned, largely in the less-populated center of the country, where it is estimated that three people died ().~~ 20. This frequent occurrence of severe bushfires, with records extending back to the 1850s, has resulted in robust preparedness and emergency management systems which serve to reduce risk and aid in swift response. Comprehensive risk assessments are undertaken at local council level, and bushfire preparedness and contingency plans have been in place in most high-risk areas for decades. However, these systems were severely strained in the Black Summer Bushfires.

7.1 Excess morbidity and mortality

The time of publication is too soon for a robust estimate of excess morbidity and mortality specific to the 2019/20 Australian Bushfires. Such analysis is typically available weeks to years following the end of an event. However, the combined impacts of extreme heat and air pollution ~~are deadly~~can be deadly, as seen in the compounded heatwave and wildfire events in 2010 in Russia or 2015 in Indonesia ((Shaposhnikov et al., 2014), Nature, 12 Aug 2010, (Koplitz et al., 2016)). Those most at risk are the elderly, people with pre-existing cardiovascular, pulmonary and/or renal conditions as well as young children~~. The 2010 wildfire and heatwave in Russia, for example, resulted in nearly 11~~, 000 excess deaths. In that event wildfires raged for three months with a 44-day heatwave occurring in parallel (Shaposhnikov et al., 2014), 300,000 hectares burned and 54 people died directly from the wildfires (,). It has also been estimated that the 2015 wildfires in Indonesia, which lasted two-months, led to approximately 100,000 excess deaths (Koplitz et al., 2016).~~

~~In addition to deaths,~~ as exposure to wildfire smoke can have acute respiratory effects. Health officials in New South Wales reported a 34% spike in emergency room visits for asthma and breathing problems between 30 December 2019 and 5 January 2020 (Washington Post, 12 Jan 2020). One study of hospital admissions in Sydney, Australia from 1994 to 2010 found that days with extreme bushfires air pollution (as measured by PM10) resulted in 1.24% admission increase for every 10 $\mu \mathrm{gm}^{-3}$ (Morgan et al., 2010). On the other hand, it should be noted that Australia is a country with a robust healthcare system which significantly reduces vulnerability to the short and long-term consequences of smoke and extreme heat.

There is also a need for increased mental health services in the days, weeks and years following ~~the~~ severe bushfires. As of January 2020 the Australian Government announced 76 million AUD in Mental Health funding (ABC, 12 January 2020). A study of the 2009 ~~Back~~ Black Saturday bushfires found that while the majority of affected people demonstrated psychological resilience in the long-term aftermath of the fires, a significant minority of people in highly affected communities reported mental health impacts 3-4 years following the event (Bryant et al., 2014).

7.2 Early Warning

There is ~~not a~~ no nationally standardized system for Bushfire Warnings in Australia. ~~. However~~However, recommendations from the Royal Commission tasked with reviewing the 2009 Victoria Bushfire (Teague et al., 2010) have helped to drive forward efforts to establish a national system. In 2014 a National Review of Warnings and Information was undertaken. It recommended the establishment of a dedicated, multi-hazard National Working Group for Public Information and Warnings. Part of the task of this group would be to ensure greater national consistency of early warning information. One outcome of this recommendation is a handbook on Public Information and Warnings which has been issued to provide guidance to actors across National, State and Territory governments in issuing warning information (AIDR, 2018).

Bushfire warnings in Australia are issued by State and Territory fire authorities and generally follow the 'Prepare, Stay and Defend or Leave Early' approach. A Fire Danger Rating system is also widely applied as a way to communicate fire risks. The system, originally developed in 1967, contained five risk levels ranging from 'low-moderate', where fires can generally be controlled, to 'extreme', where evacuation is recommended but home defence may be possible ~~if the home is located in specific places, specially designed and people have been trained on how to respond and practiced in drills~~under certain circumstances. Following the 2009 Black Saturday bushfires a sixth 'catastrophic' level was added where evacuation is deemed the only survival option (bushfire warning levels). This guidance was adopted by all states, except in Victoria where it is called 'Code Red' (BoM, 2020). In 2017, the system was revised ~~again, with an aim to improve back-end predictions by updating~~ to update the metrics used in forecasting the most appropriate level (ABC News, 12 Dec 2017). Threat level information is provided via radio, television, social media and via signs on all major rural roads. Government websites also provide information which is updated every few minutes and includes maps of fires and associated threat levels. In addition, phone calls are made house-to-house when evacuation is recommended.

While these efforts help to reduce vulnerability and exposure to the wildfires, significant barriers to early action still remain. People in bushfire areas ~~,~~are frequently not aware of their risk, unprepared to manage risk, wait until the final moments to evacuate or, at times, even return to fire affected areas to defend property ~~. (Whittaker et al., 2020)~~(Whittaker et al., 2020) . This is particularly relevant in peri-urban areas which are not as frequently exposed to bushfire risks. A 2020 study of people's reactions to bushfire warnings during the 2017 bushfires in New South Wales found that people largely understood warnings, however they did not respond to the warnings ~~in the ways intended by fire services. Consistent with other studies, researchers found that people tend to seek confirmation of the bushfire threat before evacuating, in order to avoid~~ before seeking and obtaining additional confirmation to avoid what they might perceive as unnecessary evacuation and associated ~~expenses.~~costs.. Researchers recommend that rather than further refining messages, ~~first responders need to build in confirmation mechanisms~~ confirmation mechanisms need to be implemented into early warning approaches. ~~Researchers also found that many people do not accept key messages tied to the catastrophic fire level. Specifically, people frequently do not follow recommendations to leave early, before there is a fire, and often do not believe that their house is not defendable at this level of danger (Whittaker et al., 2020). This is compounded by personal desires to keep pets and animals safe, or a determination to personally protect property in the fear that the emergency services will not succeed. There is also a 'hero '~~

culturearound those who succeed in defending their homesThere are further barriers to acting on warnings, such as an incorrect assessment of the defensibility of a building, attachments to pets and personal items, and a 'hero culture' around people who did defend their home. These sociological barriers to life-saving measures increase the risk of deadly impacts.

Furthermore, an inquiry into the 2009 Black Saturday bushfires found that the 'Prepare, Stay and Defend or Leave Early' approach assumed that individuals had a fire plan in-place, however many people did not. Therefore people were left in a position to make complex decisions without adequate guidance.

7.3 Controlled burning and relation to weather conditions

During the 2019/20 fire season, there has been wide discussion about prior fire hazard management strategies, in particular the management of vegetation cover including through bush reduction, manual removal of undergrowth and controlled burning, which is carried out by various actors, and coordinated by various authorities (mainly at state and local level). For this study, we did not assess vegetation cover and condition (dryness) ahead of the season in comparison with earlier years.–, but it is clear that fire hazard management strategies such as bush reduction, manual removal of undergrowth and controlled burning can affect fire hazard

Note that the effectiveness of such measures depends on type of vegetation, but also the specific conditions of the bushfire. For instance, prior controlled burning may be somewhat effective to suppress fire risk under average weather conditions, but much less so in cases of very high temperatures, low humidity and strong wind;, i.e., when the fire risk is no longer dominated by the type, condition and quantity of fuel but by weather conditions. For instance, for the case of the During the 2009 fires in Victoria, it was shown that recently burnt areas (up to 5–10 years) may have reduced the intensity of the fires, but not enough to increase the chance of effective suppression given the severe weather conditions at the time (Price and Bradstock, 2012).

In addition, it should be noted that controlled burning requires a window during the cooler parts of the year when conditions allow controlled burning to take place, but are not yet so volatile that controlled burning becomes too dangerous. In the case of the 2019 season in Queensland for instance, the Queensland . he Queensland Fire and Emergency Services (QFES) noted that controlled burning is highly dependent on weather conditions, and that not all planned 2019 burns had been completed, given that in some areas, it rapidly became too dry to burn safely (ABC Fact Check, 20 December 2019). Recognising the highly non-linear relationship between weather conditions through the season (and in fact across several years) and anticipatory risk management strategies, in this attribution study we have not assessed the impact of these early-season weather conditions on the ability to reduce risk, and thus on fire risk itself.

7.4 Infrastructure and land use planning

Aging electricity infrastructure may play an a role in increasing the risk of bushfire outbreaks . For example, an inquiry report following the 2009 Black Saturday bushfires estimated that 200 fires per year are started in Victoria due to the ageing electricity grid from human-related ignition(Teague et al., 2010). Electric grid fires are primarily due to elastic extension and fatigue failures, and are made increasingly worse by high wind speeds (Mitchell, 2013). A 2017 study found that fires sparked by electricity failures are more prevalent during elevated fire risk and tend to tend to burn larger, making them worse than

fires due to other causes (Miller et al., 2017). Interestingly, a 2013 report also notes that while electricity operators have the ability to disconnect electricity grids when there is a high-risk posed to the public, only South Australia has legislation in place to protect the operator from prosecution (Energy Networks Association, 2013). All of these factors coupled together increase Australia's vulnerability to bushfire outbreaks.

In contrast, stringent building codes have helped to reduce vulnerability to fire risks. The Bushfire Attack Level (BAL), and associated building codes, is the guiding resource for assessing and managing risks of a building exposed to heat, embers or direct fire. The BAL is applied nationwide, however the Fire Danger Index, one of the key metrics used in calculating the site specific BAL, is under state and local level jurisdiction. The ~~first BAL level is an indication of insufficient risk to warrant special construction requirements. There are five additional levels of potential risk, each with increasingly strict building code requirements. The highest of these requirements, BAL-FZ,~~ highest BAL level was established following the 2009 Black Saturday bushfires ~~. Illustrative examples of building restrictions at this level include window and door systems that can withstand up to 30 minutes of fire exposure and construction materials for decking, walls and roofs must be non-combustible, such as stone or bricks. Property owners can also exceed these codes by installing items like sprinkler systems, wind protection and enlarged defendable space~~ (Country Fire Authority, 2012).

~~Furthermore, land~~ Land use planning at a community level is also crucial in reducing bushfire risk, particularly for rural and ~~per-urban~~ peri-urban areas which face the highest bushfire risks. This is recognised and addressed through each state and local government planning processes, which includes ensuring accessible bushfire evacuation routes and spaces. For example, the 2009 Victorian Bushfires Royal Commission cited a need for planning which 'prioritized human life over all other policy objectives'. This led to relevant policy changes through an amendment to Victoria's Planning Provisions. The Bushfire Management Overlay, and associated guidelines, are among the principle aspects of this amendment. They provide direction for approval of new construction locations as well as siting and layout requirements of approved spaces, although these guidelines do not apply to existing property which puts a limitation on their overall positive impact (Country Fire Authority, 2012).

7.5 ~~Volunteer fire response~~

~~The Australian states of Victoria, New South Wales, South Australia and Western Australia rely on a century-old model of volunteer fire services to combat bushfires. This model has historically worked due to the episodic and fragmented nature of bushfires in Australia. In the 2019/20 bushfire season the dedication of this volunteer force saved countless lives and reduced what could have been significantly larger impacts. This largely unparalleled volunteer force is a crucial asset to managing bushfire response in Australia. For example, the New South Wales Rural Fire Service has over 72,000 volunteer fire responders, roughly 900 paid staff and provides emergency fire services to 95% of New South Wales ().~~

~~However the intensity and longevity of the 2019/20 bushfires has also raised questions regarding the sustainability of the current volunteer fire response model in a changing climate. During this bushfire season, volunteers faced long hours and extended periods of leave, in many cases depleting their various forms of paid time-off, and/or taking leave without pay. In the case of unemployed volunteers who were receiving social security benefits, a waiver mechanism was activated for 13 weeks to avoid benefit cuts due to not being able to attend job interviews and complete other required processes (). In the case of New~~

~~South Wales for example many volunteers exceeded 100 days of volunteer service, which can take a significant toll financially as well as from a physical and mental health perspective (). In December 2019, federal employees were made eligible for four weeks of paid leave and, following political pressure, compensation was extended to non-Federal employees for up to 20 days. While this compensation helps, questions remain regarding how to bolster this volunteer force as Australia's bushfire seasons become longer and more intense. Proposals include formalising compensation schemes, provision of professional training, emergency driving tests, physical fitness tests and increased budget allocations for protective equipment (as many volunteers buy their own).~~

7.5 Conclusions vulnerability and exposure

Bushfires are a natural phenomenon, but their impact is also strongly influenced by human choices. ~~The bushfire warning system in place in Australia worked well, but research shows that many people do not heed warnings in the ways intended. The risk of bushfires also includes many other anthropogenic factors, for instance increasing risk due to aging electricity infrastructure, and risk reduction for instance through building codes and land use planning. The effectiveness of some risk management options to mitigate against bushfire risk, such as using controlled burning, can also be affected by weather conditions. And some systems to respond, such as voluntary fire response, may come under strain under extreme conditions such as this fire season. Overall, however,~~ Overall, Australia is one of the most prepared countries in the world to manage bushfires and thus the impacts from this season's bushfire outbreaks could have been dramatically worse if not for the systems in place. This underscores the urgent need to adapt to changing risks in all places, with a special focus on the most vulnerable, but also highlights the limits to risk reduction and preparedness.

As a result of the Black Summer bushfires, formal inquiries have been launched in Victoria (Victoria Government, 14 Jan 2020), New South Wales(New South Wales Government, Jan 2020), Queensland (Queensland Government, 18 Dec 2019) and South Australia (South Australia Government, 21 Jan 2020). A Federal Royal Commission has ~~also~~ been announced with an aim to improve resilience, preparedness and response to disasters across all levels of government. The Commission will also seek to improve disaster management coordination across local government ~~,~~ and improve relevant legal frameworks. These inquiries will ~~undoubtedly~~ shed additional light on the vulnerability and exposure elements of the Black Summer Bushfires, and hopefully help mitigate future risk.

8 Conclusions

We investigated changes in the risk of bushfire weather in southeastern Australia due to anthropogenic climate change, underpinned by changes in extreme heat and extreme drought. The latter have longer time series and are covered by many more climate models, leading to more robust conclusions. The fire risk is described by the Fire Weather Index, which was shown to correlate well with the area burnt in this part of Australia.

The first conclusion is that current climate models struggle to represent extremes in the 7-day averaged maximum temperature which was chosen as the most impact-relevant definition of heat as well as the Fire Weather Index. They tend to

overestimate variability and thus underestimate the observed trends in these variables. Both of these factors give an underestimation of the change in probability due to anthropogenic climate change (PR). We therefore do not give best fit values but only lower bounds for these variables.

We find that the probability of extreme heat has increased by at least a factor two. We do not find attributable trends in extreme drought, neither on the annual time scale nor for the driest month in the fire season, even when mean precipitation does have drying trends in some models. Commensurate with this we find a significant increase in the risk of fire weather as severe or worse as observed in 2019/20 by at least 30%. Both for extreme heat and fire weather we think the true ~~chance~~ change in probability is likely much higher due to the model deficiencies.

The fire weather of 2019 was made much more severe by record positive excursions of the Indian Ocean dipole, even when the ENSO teleconnection was removed from this. The average effect of this mode is small, but the anomaly was so large that this factor explains about one third of the anomalous drought in July–December 2019. The other factor was the Southern Annular Mode, which was also ~~anomalous~~ anomalously negative during this time, explaining another one third of the July–December drought. Both factors were predicted well and gave good warning of the high fire risk in late 2019. The variability due to these modes is included in our analysis, although the simulated fidelity of the modes themselves and their trends has not been assessed in detail here. It should be noted that only a small fraction of the natural variability is described by these modes.

Of course the full fire risk is also affected by non-weather factors. The bushfire warning system in place in Australia worked well, but research shows that many people do not follow the guidelines as intended. The risk of bushfires is increased due to anthropogenic factors like aging electricity infrastructure. Efforts to mitigate against that risk using controlled burning are hampered by the very high fire risk due to weather factors shrinking the window in which controlled burning can be safely executed. Overall, however, Australia is one of the most prepared countries in the world to manage bushfires and thus the impacts from this season's bushfire outbreaks could have been dramatically worse if not for the systems in place. This underscores the urgent need to adapt to changing risks in all places, and especially the most vulnerable.

Although we clearly identify a connection between climate change and fire weather and ascertain a lower bound, we also find, in agreement with other studies, that we need more understanding of the biases in climate models and their resolution before we can make a more quantitative statement of how strong the connection is and how it will evolve in the future. Ever more detailed attribution statements are desired by society and scientific progress in the modelling of extreme events is therefore needed.

Data availability

Almost all data used in the analyses can be downloaded from the KNMI Climate Explorer at https://climexp.knmi.nl/bushfires_timeseries.cgi. This also contains the scripts that we used to do all the extreme value fits. These can also be performed using the graphical user interface of the Climate Explorer.

Acknowledgements. We thank Pandora Hope, Andrew Dowdy and Mitchell Black of the Bureau of Meteorology and Sarah Perkins-Kirkpatrick of the University of New South Wales for substantial contributions to the article. G.J.v.O was supported by the ERA4CS projects SERV_FORFIRE and EUPHEME (grant #690462). The contribution of F. K. was supported by the Belmont Forum Project PREREAL (grant # 292-2015-11-30-13-43-09 to I.D.). F.L. is supported by the Regional and Global Model Analysis (RGMA) component of the Earth and Environmental System Modeling Program of the US Department of Energy's Office of Biological & Environmental Research (BER) via NSF IA 1947282, and by a Swiss NSF Ambizione Fellowship (Project PZ00P2_174128). We acknowledge the use of data and imagery from LANCE FIRMS operated by NASA's Earth Science Data and Information System (ESDIS) with funding provided by NASA Headquarters. We would like to thank all the volunteers who have donated their computing time to climateprediction.net and weather@home.

References

Abatzoglou, J. T., Williams, A. P., and Barbero, R.: Global Emergence of Anthropogenic Climate Change in Fire Weather Indices, Geophysical Research Letters, 46, 326–336, https://doi.org/10.1029/2018GL080959, 2019.

Agard, J., Schipper, E. L. F., et al., eds.: AR5 Climate Change 2014: Impacts, Adaptation, and Vulnerability: Annex II Glossary, Cambridge University Press, New York, 2014.

Black, M. T., Karoly, D. J., and King, A. D.: The contribution of anthropogenic forcing to the Adelaide and Melbourne, Australia, heat waves of January 2014, Bull. Amer. Met. Soc., 96, S145–S148, https://doi.org/10.1175/BAMS-D-15-00097.1, 2015.

Boucher, O., Servonnat, J., Albright, A. L., Aumont, O., Y., B., Bastriko, V., Bekki, S., Bonnet, R., Bony, S., Bopp, L., Braconnot, P., Brockmann, P., Cadule, P., Caubel, A., Cheru, F., Cozic, A., Cugnet, D., D'Andrea, F., Davini, P., de Lavergne, C., Denvil, S., Deshayes, J., M., D., Ducharne, A., Dufresne, J.-L., Dupont, E., Ethé, C., Fairhead, L., Falletti, L., Foujols, M.-A., Gardoll, S., Gastinea, G., J., G., Grandpeix, J.-Y., Guenet, B., Guez, L., Guilyardi, E., Guimberteau, M., Hauglustaine, D., Hourdin, F., Idelkadi, A., Joussaume, S., Kageyama, M., Khadre-Traoré, A., Khodri, M., Krinner, G., Lebas, N., Levavasseur, G., Lévy, C., Li, L., Lott, F., Lurton, T., Luyssaert, S., G., M., Madeleine, J.-B., Maignan, F., Marchand, M., Marti, O., Mellul, L., Meurdesoif, Y., Mignot, J., Musat, I., Ottlé, C., Peylin, P., Planton, Y., Polcher, J., Rio, C., Rousset, C., Sepulchre, P., Sima, A., Swingedouw, D., Thieblemont, R., Traoré, A., Vancoppenolle, M., Vial, J., Vialard, J., Viovy, N., and Vuichard, N.: Presentation and evaluation of the IPSL-CM6A-LR climate model, J. Adv. Modeling Earth Systems, submitted, 2020.

Bryant, R. A., Waters, E., Gibbs, L., Gallagher, H. C., Pattison, P., Lusher, D., MacDougall, C., Harms, L., Block, K., Snowdon, E., Sinnott, V., Ireton, G., Richardson, J., and Forbes, D.: Psychological outcomes following the Victorian Black Saturday bushfires, Australian & New Zealand Journal of Psychiatry, 48, 634–643, https://doi.org/10.1177/0004867414534476, pMID: 24852323, 2014.

Camia, A. and Amatulli, G.: Weather Factors and Fire Danger in the Mediterranean, in: Earth Observation of Wildland Fires in Mediterranean Ecosystems, edited by Chuvieco, Springer, Berllin, Heidelberg, https://doi.org/10.1007/978-3-642-01754-4_6, 2009.

Ciavarella, A., Christidis, N., Andrews, M., Groenendijk, M., Rostron, J., Elkington, M., Burke, C., Lott, F. C., and Stott, P. A.: Upgrade of the HadGEM3-A based attribution system to high resolution and a new validation framework for probabilistic event attribution, Weather and Climate Extremes, 20, 9 – 32, https://doi.org/10.1016/j.wace.2018.03.003, 2018.

Clarke, H., Lucas, C., and Smith, P.: Changes in Australian fire weather between 1973 and 2010, Int. J. Climatol., 33, 931–944, https://doi.org/10.1002/joc.3480, 2013.

Clarke, H. G., Smith, P. L., and Pitman, A. J.: Regional signatures of future fire weather over eastern Australia from global climate models, International Journal of Wildland Fire, 20, 550–562, 2011.

Coles, S.: An Introduction to Statistical Modeling of Extreme Values, Springer Series in Statistics, London, UK, 2001.

Cooley, D., Hunter, B., and Smith, R.: Univariate and multivariate extremes for the environmental sciences, Environmental Statistics, pp. 153–180, 2018.

Country Fire Authority: Planning for Bushfire Victoria, version 2, https://www.eastgippsland.vic.gov.au/files/content/public/planning_and_building/planning_reference_and_incorporated_documents/reference_documents/cfa_planning_conditions_guidelines_amended.pdf, 2012.

Dimitrakopoulos, A. P., Bemmerzouk, A. M., and Mitsopoulos, I. D.: Evaluation of the Canadian fire weather index system in an eastern Mediterranean environment, Meteorological Applications, 18, 83–93, https://doi.org/10.1002/met.214, 2011.

Dowdy, A. J.: Climatological Variability of Fire Weather in Australia, Journal of Applied Meteorology and Climatology, 57, 221–234, https://doi.org/10.1175/JAMC-D-17-0167.1, 2018.

Dowdy, A. J. and Pepler, A.: Pyroconvection Risk in Australia: Climatological Changes in Atmospheric Stability and Surface Fire Weather Conditions, Geophys. Res. Lett., 45, 2005–2013, https://doi.org/10.1002/2017GL076654, 2018.

Dowdy, A. J., Mills, G. A., Finkele, K., and de Groot, W.: Australian fire weather as represented by the McArthur Forest Fire Danger Index and the Canadian Forest Fire Weather Index, Technical Report 10, The Centre for Australian Weather and Climate Research, 2009.

Dowdy, A. J., Ye, H., Pepler, A., Thatcher, M., Osbrough, S. L., Evans, J. P., Di Virgilio, G., and McCarthy, N.: Future changes in extreme weather and pyroconvection risk factors for Australian wildfires, Scientific Reports, 9, 10 073, https://doi.org/10.1038/s41598-019-46362-x, 2019.

Eden, J. M., Wolter, K., Otto, F. E. L., and van Oldenborgh, G. J.: Multi-method attribution analysis of extreme precipitation in Boulder, Colorado, Environ. Res. Lett., 11, 124 009, https://doi.org/10.1088/1748-9326/11/12/124009, 2016.

Eden, J. M., Kew, S. F., Bellprat, O., Lenderink, G., Manola, I., Omrani, H., and van Oldenborgh, G. J.: Extreme precipitation in the Netherlands: An event attribution case study, Weather and Climate Extremes, 21, 90–101, https://doi.org/10.1016/j.wace.2018.07.003, 2018.

Energy Networks Association: Bushfires + Energy Networks, https://www.energynetworks.com.au/resources/fact-sheets/bushfires-and-energy-networks/, 2013.

Finlay, S. E., Moffat, A., Gazzard, R., Baker, D., and Murray, V.: Health impacts of wildfires, PLoS Currents Disasters, 4, e4f959 951cce2c, https://doi.org/10.1371/4f959951cce2c, 2012.

Fischer, E. M., Seneviratne, S. I., Vidale, P. L., Lüthi, D., and Schär, C.: Soil Moisture–Atmosphere Interactions during the 2003 European Summer Heat Wave, Journal of Climate, 20, 5081–5099, https://doi.org/10.1175/JCLI4288.1, 2007.

Guillod, B. P., Jones, R. G., Bowery, A., Haustein, K., Massey, N. R., Mitchell, D. M., Otto, F. E. L., Sparrow, S. N., Uhe, P., Wallom, D. C. H., Wilson, S., and Allen, M. R.: weather@home 2: validation of an improved global–regional climate modelling system, Geoscientific Model Development, 10, 1849–1872, https://doi.org/10.5194/gmd-10-1849-2017, 2017.

Haikerwal, A., Akram, M., Del Monaco, A., Smith, K., Sim, M. R., Meyer, M., Tonkin, A. M., Abramson, M. J., and Dennekamp, M.: Impact of Fine Particulate Matter (PM2.5) Exposure During Wildfires on Cardiovascular Health Outcomes, Journal of the American Heart Association, 4, e001 653, https://doi.org/10.1161/JAHA.114.001653, 2015.

Hansen, J., Ruedy, R., Sato, M., and Lo, K.: Global Surface Temperature Change, Rev. Geophys., 48, RG4004, https://doi.org/DOI 10.1029/2010RG000345, 2010.

Harris, S. and Lucas, C.: Understanding the variability of Australian fire weather between 1973 and 2017, PLoS ONE, 14, e0222 328, https://doi.org/10.1371/journal.pone.0222328, 2019.

Haustein, K., Otto, F. E. L., Venema, V., Jacobs, P., Cowtan, K., Hausfather, Z., Way, R. G., White, B., Subramanian, A., and Schurer, A. P.: A Limited Role for Unforced Internal Variability in Twentieth-Century Warming, J. Climate, 32, 4893–4917, https://doi.org/10.1175/JCLI-D-18-0555.1, 2019.

Hazeleger, W., Severijns, C., Semmler, T., Stefanescu, S., Yang, S., Wang, X., Wyser, K., Dutra, E., Baldasano, J. M., Bintanja, R., Bougeault, P., Caballero, R., Ekman, A. M. L., Christensen, J. H., van den Hurk, B., Jimenez, P., Jones, C., Kallberg, P., Koenigk, T., McGrath, R., Miranda, P., Van Noije, T., Palmer, T., Parodi, J. A., Schmith, T., Selten, F., Storelvmo, T., Sterl, A., Tapamo, H., Vancoppenolle, M., Viterbo, P., and Willen, U.: EC-Earth: A Seamless Earth-System Prediction Approach in Action, Bull. Amer. Met. Soc., 91, 1357–1363, https://doi.org/DOI 10.1175/2010BAMS2877.1, 2010.

Hersbach, H., Bell, W., Berrisford, P., Horányi, A., J., M.-S., Nicolas, J., Radu, R., Schepers, D., Simmons, A., Soci, C., and Dee, D.: Global reanalysis: goodbye ERA-Interim, hello ERA5, ECMWF Newsletter, 159, 17–24, https://doi.org/10.21957/vf291hehd7, 2019.

Hope, P., Wang, G., Lim, E.-P., Hendon, H. H., and Arblaster, J. M.: What caused the recofrd-breaking heat across Australia in October 2015?, Bull. Amer. Met. Soc., 97, S1–S5, https://doi.org/10.1175/BAMS-D-16-0142.1, 2016.

Hope, P., Black, M. T., Lim, E.-P., Dowdy, A., Wang, G., Pepler, A. S., and Fawcett, R. J. B.: On Determining the Impact of Increasing Atmospheric CO2 on the Record Fire Weather In Eastern Australia In February 2017, Bull. Amer. Met. Soc., 100, S111–S117, https://doi.org/10.1175/BAMS-D-18-0135.1, 2019.

Jeffrey, S., Rotstayn, L., Collier, M., Dravitzki, S., Hamalainen, C., Moeseneder, C., Wong, K., and Syktus, J.: Australia's CMIP5 submission using the CSIRO-Mk3. 6 model, Aust. Meteor. Oceanogr. J, 63, 1–13, 2013.

Johnston, F. and Bowman, D.: Bushfire Smoke: An Exemplar of Coupled Human and Natural Systems, Geographical Research, 52, 45–54, https://doi.org/10.1111/1745-5871.12028, 2014.

Kala, J., De Kauwe, M. G., Pitman, A. J., Medlyn, B. E., Wang, Y.-P., Lorenz, R., and Perkins-Kirkpatrick, S. E.: Impact of the representation of stomatal conductance on model projections of heatwave intensity, Scientific Reports, 6, 23 418, https://doi.org/10.1038/srep23418, 2016.

Kay, J. E., Deser, C., Phillips, A., Mai, A., Hannay, C., Strand, G., Arblaster, J. M., Bates, S., Danabasoglu, G., Edwards, J., et al.: The Community Earth System Model (CESM) large ensemble project: A community resource for studying climate change in the presence of internal climate variability, Bulletin of the American Meteorological Society, 96, 1333–1349, https://doi.org/10.1175/BAMS-D-13-00255.1, 2015.

Kew, S. F., Philip, S. Y., van Oldenborgh, G. J., Otto, F. E., Vautard, R., and van der Schrier, G.: The exceptional summer heatwave in Southern Europe 2017, Bull. Amer. Met. Soc., 100, S2–S5, https://doi.org/10.1175/BAMS-D-18-0109.1, 2019.

King, A. D., Black, M. T., Karoly, D. J., and Donat, M. G.: Incraesed likelihood of Brisbane, Australia, G20 heat event due to anthropogenic climate change, Bull. Amer. Met. Soc., 96, S141–S144, https://doi.org/10.1175/BAMS-D-15-00098.1, 2015a.

King, A. D., van Oldenborgh, G. J., Karoly, D. J., Lewis, S. C., and Cullen, H.: Attribution of the record high Central England temperature of 2014 to anthropogenic influences, Environmental Research Letters, 10, 054 002, https://doi.org/10.1088/1748-9326/10/5/054002, 2015b.

King, A. D., van Oldenborgh, G. J., and Karoly, D. J.: Climate Change and El Niño increase likelihood of Indonesian heat and drought, Bull. Amer. Met. Soc., 97, S113–S117, https://doi.org/10.1175/BAMS-D-16-0164.1, 2016.

Kirchmeier-Young, M. C., Zwiers, F. W., and Gillett, N. P.: Attribution of extreme events in Arctic sea ice extent, Journal of Climate, 30, 553–571, https://doi.org/10.1175/JCLI-D-16-0412.1, 2017.

Koplitz, S. N., Mickley, L. J., Marlier, M. E., Buonocore, J. J., Kim, P. S., Liu, T., Sulprizio, M. P., DeFries, R. S., Jacob, D. J., Schwartz, J., Pongsiri, M., and Myers, S. S.: Public health impacts of the severe haze in Equatorial Asia in September–October 2015: demonstration of a new framework for informing fire management strategies to reduce downwind smoke exposure, Environ. Res. Lett., 11, 094 023, https://doi.org/10.1088/1748-9326/11/9/094023, 2016.

Krikken, F., Lehner, F., Haustein, K., Drobyshev, I., and van Oldenborgh, G. J.: Attribution of the role of climate change in the forest fires in Sweden 2018, Natural Hazards and Earth System Sciences Discussions, 2019, 1–24, https://doi.org/10.5194/nhess-2019-206, 2019.

Lewis, S., Blake, S., Trewin, B., Black, M., Dowdy, A., Perkins-Kirkpatrick, S., King, A., and Sharples, J.: Deconstructing factors contributing to the 2018 fire weather in Queensland, Australia, Bull. Amer. Met. Soc., https://doi.org/10.1175/BAMS-D-19-0144.1, 2019.

Lewis, S. C. and Karoly, D. J.: Anthropogenic contributions to Australia's record summer temperatures of 2013, Geophysical Research Letters, 40, 3705–3709, https://doi.org/10.1002/grl.50673, 2013.

Maher, N., Milinski, S., Suarez-Gutierrez, L., Botzet, M., Kornblueh, L., Takano, Y., Kröger, J., Ghosh, R., Hedemann, C., Li, C., et al.: The Max Planck Institute grand ensemble-enabling the exploration of climate system variability, Journal of Advances in Modeling Earth Systems, 11, 2050–2069, https://doi.org/10.1029/2019MS001639, 2019.

Martins, E. S. P. R., Coelho, C. A. S., Haarsma, R. J., Otto, F. E. L., King, A. D., van Oldenborgh, G. J., Kew, S. F., Philip, S. Y., Vasconselos Junior, F. C., and Cullen, H.: A multimethod attribution analysis of the prolonged northeast Brazil hydrometeorological drought (2012–16), Bull. Amer. Met. Soc., 99, S65–S69, https://doi.org/10.1175/BAMS-D-17-0102.1, 2018.

Mathur, R. and AchutaRao, K.: A modelling exploration of the sensitivity of the India's climate to irrigation, Climate Dynamics, https://doi.org/10.1007/s00382-019-05090-8, 2019.

McArthur, A. G.: Weather and grassland fire behaviour, Tech. Rep. Leaflet 100, Aust. For. Timb. Bur., 1966.

McArthur, A. G.: Fire behaviour in eucalypt forest, Tech. Rep. Leaflet 107, Aust. For. Timb. Bur., 1967.

Miller, C., Plucinski, M., Sullivan, A., Stephenson, A., Huston, C., Charman, K., Prakash, M., and Dunstall, S.: Electrically caused wildfires in Victoria, Australia are over-represented when fire danger is elevated, Landscape and Urban Planning, 167, 267 – 274, https://doi.org/10.1016/j.landurbplan.2017.06.016, 2017.

Miralles, D. G., Teuling, A. J., van Heerwaarden, C. C., and Vilà-Guerau de Arellano, J.: Mega-heatwave temperatures due to combined soil desiccation and atmospheric heat accumulation, Nature Geoscience, 7, 345–349, https://doi.org/10.1038/ngeo2141, 2014.

Mitchell, J. W.: Power line failures and catastrophic wildfires under extreme weather conditions, Engineering Failure Analysis, 35, 726–735, https://doi.org/10.1016/j.engfailanal.2013.07.006, special issue on ICEFA V- Part 1, 2013.

Morgan, G., Sheppeard, V., Khalaj, B., Ayyar, A., Lincoln, D., Jalaludin, B., Beard, J., Corbett, S., and Lumley, T.: Effects of Bushfire Smoke on Daily Mortality and Hospital Admissions in Sydney, Australia, Epidemiology, 21, 47–55, https://doi.org/10.1097/EDE.0b013e3181c15d5a, 2010.

Naveau, P., Huser, R., Ribereau, P., and Hannart, A.: Modeling jointly low, moderate, and heavy rainfall intensities without a threshold selection, Water Resources Research, 52, 2753–2769, 2016.

Noble, I. R., Gill, A. M., and Bary, G. A. V.: McArthur's fire-danger meters expressed as equations, Australian Journal of Ecology, 5, 201–203, https://doi.org/10.1111/j.1442-9993.1980.tb01243.x, 1980.

Otto, F. E. L., van der Wiel, K., van Oldenborgh, G. J., Philip, S. Y., Kew, S. F., Uhe, P., and Cullen, H.: Climate change increases the probability of heavy rains in Northern England/Southern Scotland like those of storm Desmond—a real-time event attribution revisited, Environ. Res. Lett., 13, 024 006, https://doi.org/10.1088/1748-9326/aa9663, 2018a.

Otto, F. E. L., Wolski, P., Lehner, F., Tebaldi, C., van Oldenborgh, G. J., Hogesteeger, S., Singh, R., Holden, P., Fuckar, N. S., Odoulami, R., and New, M.: Anthropogenic influence on the drivers of the Western Cape drought 2015–2017, Environ. Res. Lett., 13, 124 010, https://doi.org/10.1088/1748-9326/aae9f9, 2018b.

Pasquale, C.: Are your data really Pareto distributed?, Physica A: Statistical Mechanics and its Applications, 392, 5947–5962, https://doi.org/10.1016/j.physa.2013.07.061, 2013.

Pepler, A., Coutts-Smith, A., and Timbal, B.: The role of East Coast Lows on rainfall patterns and inter-annual variability across the East Coast of Australia, Int. J. Climatol., 34, 1011–1021, https://doi.org/10.1002/joc.3741, 2014.

Perkins, S. E. and Gibson, P. B.: Increased risk of the 2014 Australian May heatwave due to anthrpogenic activity, Bull. Amer. Met. Soc., 96, S154–S157, https://doi.org/10.1175/BAMS-D-15-00074.1, 2015.

Perkins, S. E., Lewis, S. C., King, A. D., and Alexander, L. V.: Increased Simulated Risk of the Hot Australian Summer of 2012/13 due to Anthropogenic Activity as Measured by Heat Wave Frequency and Intensity, Bull. Amer. Met. Soc., 95, S34–S37, 2014.

Philip, S. Y., Kew, S. F., Hauser, M., Guillod, B. P., Teuling, A. J., Whan, K., Uhe, P., and Oldenborgh, G. J. v.: Western US high June 2015 temperatures and their relation to global warming and soil moisture, Clim. Dyn., 50, 2587–2601, https://doi.org/10.1007/s00382-017-3759-x, 2018a.

Philip, S. Y., Kew, S. F., van Oldenborgh, G. J., Aalbers, E., Otto, F. E. L., Haustein, K., Habets, F., and Singh, R.: Validation of a rapid attribution of the May/June 2016 flood-inducing precipitation in France to climate change, Journal of Hydrometeorology, 19, 1881–1898, https://doi.org/10.1175/JHM-D-18-0074.1, 2018b.

Philip, S. Y., Kew, S. F., van Oldenborgh, G. J., Otto, F. E. L., O'Keefe, S., Haustein, K., King, A. D., Zegeye, A., Eshetu, Z., Hailemariam, K., Singh, R. K., Jjemba, E., Funk, C., and Cullen, H.: Attribution analysis of the Ethiopian drought of 2015, J. Climate, 31, 2465–2486, https://doi.org/10.1175/JCLI-D-17-0274.1, 2018c.

Philip, S. Y., Kew, S. F., van Oldenborgh, G. J., Otto, F. E. L., Vautard, R., van der Wiel, K., King, A. D., Lott, F. C., Arrighi, J., Singh, R. P., and van Aalst, M. K.: A protocol for probabilistic extreme event attribution analyses, Advances in Statistical Climatology, Meteorology and Oceanography, 6, 177–203, https://doi.org/10.5194/ascmo-6-177-2020, 2020.

Price, O. F. and Bradstock, R. A.: The efficacy of fuel treatment in mitigating property loss during wildfires: Insights from analysis of the severity of the catastrophic fires in 2009 in Victoria, Australia, Journal of Environmental Management, 113, 146 – 157, https://doi.org/10.1016/j.jenvman.2012.08.041, 2012.

Reid, C. E., Brauer, M., Johnston, F. H., Jerrett, M., Balmes, J. R., and Elliott, C. T.: Critical Review of Health Impacts of Wildfire Smoke Exposure, Environmental Health Perspectives, 124, 1334–1343, https://doi.org/10.1289/ehp.1409277, 2016.

Ribes, A., Thao, S., and Cattiaux, J.: Describing the Relationship between a Weather Event and Climate Change: A New Statistical Approach, Journal of Climate, 33, 6297–6314, https://doi.org/10.1175/JCLI-D-19-0217.1, 2020.

Rodgers, K. B., Lin, J., and Frölicher, T. L.: Emergence of multiple ocean ecosystem drivers in a large ensemble suite with an Earth system model, Biogeosciences, 12, 3301–3320, https://doi.org/10.5194/bg-12-3301-2015, 2015.

Sanderson, B. M. and Fisher, R. A.: A fiery wake-up call for climate science, Nature Climate Change, https://doi.org/10.1038/s41558-020-0707-2, 2020.

Schaller, N., Otto, F. E. L., van Oldenborgh, G. J., Massey, N. R., Sparrow, S., and Allen, M. R.: The heavy precipitation event of May–June 2013 in the upper Danube and Elbe basins, Bull. Amer. Met. Soc., 95, S69–S72, 2014.

Shabbar, A., Skinner, W., and Flannigan, M. D.: Prediction of Seasonal Forest Fire Severity in Canada from Large-Scale Climate Patterns, Journal of Applied Meteorology and Climatology, 50, 785–799, https://doi.org/10.1175/2010JAMC2547.1, 2011.

Shaposhnikov, D., Revich, B., Bellander, T., Bedada, G. B., Bottai, M., Kharkova, T., Kvasha, E., Lezina, E., Lind, T., Semutnikova, E., and Pershagen, G.: Mortality related to air pollution with the moscow heat wave and wildfire of 2010, Epidemiology (Cambridge, Mass.), 25, 359–364, https://doi.org/10.1097/EDE.0000000000000090, 2014.

Siswanto, van Oldenborgh, G. J., van der Schrier, G., Lenderink, G., and van den Hurk, B. J. J. M.: Trends in high-daily precipitation events in Jakarta and the flooding of January 2014, Bull. Amer. Met. Soc., 96, S131–S135, https://doi.org/10.1175/BAMS-D-15-00128.1, 2015.

Sun, L., Alexander, M., and Deser, C.: Evolution of the global coupled climate response to Arctic sea ice loss during 1990–2090 and its contribution to climate change, Journal of Climate, 31, 7823–7843, https://doi.org/10.1175/JCLI-D-18-0134.1, 2018.

Teague, B., McLeod, R., and Pascoe, S.: 2009 Victorian Bushfires Royal Commission Report (Summary), iSBN 978-0-9807408-1-3, http://royalcommission.vic.gov.au/finaldocuments/summary/PF/VBRC_Summary_PF.pdf, 2010.

Tebaldi, C. and Arblaster, J. M.: Pattern scaling: Its strengths and limitations, and an update on the latest model simulations, Climatic Change, 122, 459–471, https://doi.org/10.1007/s10584-013-1032-9, 2014.

Thiery, W., Davin, E. L., Lawrence, D. M., Hirsch, A. L., Hauser, M., and Seneviratne, S. I.: Present-day irrigation mitigates heat extremes, Journal of Geophysical Research: Atmospheres, 122, 1403–1422, https://doi.org/10.1002/2016JD025740, 2017.

Uhe, P., Philip, S. Y., Kew, S. F., Shah, K., Kimutai, J., Mwangi, E., van Oldenborgh, G. J., Singh, R. K., Arrighi, J., Jjemba, E., Cullen, H., and Otto, F. E. L.: Attributing drivers of the 2016 Kenyan drought, Int. J. Climatol., 38, e554–e568, https://doi.org/10.1002/joc.5389, 2018.

van der Wiel, K., Kapnick, S. B., van Oldenborgh, G. J., Whan, K., Philip, S. Y., Vecchi, G. A., Singh, R. K., Arrighi, J., and Cullen, H.: Rapid attribution of the August 2016 flood-inducing extreme precipitation in south Louisiana to climate change, Hydrol. Earth Syst. Sci., 21, 897–921, https://doi.org/10.5194/hess-21-897-2017, 2017.

van Oldenborgh, G. J., Haarsma, R., De Vries, H., and Allen, M. R.: Cold Extremes in North America vs. Mild Weather in Europe: The Winter of 2013–14 in the Context of a Warming World, Bulletin of the American Meteorological Society, 96, 707–714, https://doi.org/10.1175/BAMS-D-14-00036.1, 2015.

van Oldenborgh, G. J., Otto, F. E. L., Haustein, K., and Achuta Rao, K.: The heavy precipitation event of December 2015 in Chennai, India, Bull. Amer. Met. Soc., 97, S87–S91, https://doi.org/10.1175/BAMS-D-16-0129.1, 2016.

van Oldenborgh, G. J., van der Wiel, K., Sebastian, A., Singh, R. K., Arrighi, J., Otto, F. E. L., Haustein, K., Li, S., Vecchi, G. A., and Cullen, H.: Attribution of extreme rainfall from Hurricane Harvey, August 2017, Environ. Res. Lett., 12, 124 009, https://doi.org/10.1088/1748-9326/aa9ef2, 2017.

van Oldenborgh, G. J., Philip, S. Y., Kew, S. F., van Weele, M., Uhe, P., Otto, F. E. L., Singh, R. K., Pai, I., Cullen, H., and AchutaRao, K.: Extreme heat in India and anthropogenic climate change, Natural Hazards and Earth System Sciences, 18, 365–381, https://doi.org/10.5194/nhess-18-365-2018, 2018.

Van Wagner, C. E.: Conversion of William's Severity Rating for Use with the Fire Weather Index, Petawawa For. Exp. Sta. Inf. Rep. PS-X-21, Can. For. Serv., 1970.

Vautard, R., van Oldenborgh, G. J., Thao, S., Dubuisson, B., Lenderink, G., Ribes, A., Soubeyroux, J. M., Yiou, P., and Planton, S.: Extreme fall 2014 precipitations in the Cévennes mountain range, Bull. Amer. Meteor. Soc., 96, S56–S60, https://doi.org/10.1175/BAMS-D-15-00088.1, 2015.

Weisheimer, A., Schaller, N., O'Reilly, C., MacLeod, D. A., and Palmer, T.: Atmospheric seasonal forecasts of the twentieth century: multi-decadal variability in predictive skill of the winter North Atlantic Oscillation (NAO) and their potential value for extreme event attribution, Quarterly Journal of the Royal Meteorological Society, 143, 917–926, https://doi.org/10.1002/qj.2976, 2017.

Whittaker, J., Taylor, M., and Bearman, C.: Why don't bushfire warnings work as intended? Responses to official warnings during bushfires in New South Wales, Australia, International Journal of Disaster Risk Reduction, 45, 101 476, https://doi.org/https://doi.org/10.1016/j.ijdrr.2020.101476, 2020.